FAR-INFRARED RADIATIVE PROPETIES OF SUPERCONDUCTING YBCO FILMS DEPOSITED ON SILICON SUBSTRATES

By

RAVI KUMAR ADIMULA

A DISSERTATION PRESENTED TO THE GRADUATE SCHOOL
OF THE UNIVERSITY OF FLORIDA IN PARTIAL FULFILLMENT
OF THE REQUIREMENTS FOR THE DEGREE OF
DOCTOR OF PHILOSOPHY

UNIVERSITY OF FLORIDA

1999

ACKNOWLEDGMENTS

I take this opportunity to thank my advisor, Dr. Zhuomin Zhang, for his constant encouragement, valuable guidance and support. He was always helpful in meeting the requirements under great time constraints and provided assistance beyond this research work. Professor David Tanner has been a great source of information throughout this project. I sincerely thank him for allowing me to use his lab facilities and for teaching some valuable experimental techniques. I sincerely thank Drs. David Rudman and Leila Vale of NIST for providing good quality sample films used in this project. I also would like to thank Drs. Jacob Chung, Yogi Goswami, David Hahn, and Jill Peterson for serving on my supervisory committee.

I am very grateful to Vladimir Boychev for his assistance in conducting experiments at all stages of the project. I appreciate the help provided by Akito Ugawa and Lev Gasparov at different stages of experiments. Association with Brian Johnson, Donghai Chen, Ferdinand Rosa and Yu-Jiun Shen helped in learning a lot about different cultures and traditions. David Pearson will always remain a truly endearing companion. My stay at UF is memorable thanks to many good friends I had. My obsession with political and economic issues was truly matched by my good friend Uday. I will always remember all those *Corona* discussions I had with Uday on all those wide ranging topics.

I am grateful to the financial and moral support provided by my sister Rajeswari and her husband Chandra Sekhar, without which I would not have made it this far in my life. I also thank my mother for her love and affection.

Final thanks go to the supporters of this project: University of Florida through an Interdisciplinary Research Initiative (IRI) award and the National Science Foundation through grant CTS-9812027.

TABLE OF CONTENTS

page

ACKNOWLEDGMENTS ii

NOMENCLATURE v

ABSTRACT vii

CHAPTERS

1 INTRODUCTION 1

2 APPLICATIONS OF HTSC FILMS AND PREVIOUS STUDIES 4

Some Potential Applications of HTSC Thin Films 4
Infrared Studies on HTSC Films 8

3 THEORETICAL CONSIDERATIONS 15

Electrical Conductivity 15
Dielectric Functions 18
Radiative Properties of Multilayers 22

4 EXPERIMENTS 34

Far-Infrared Measurements 34
YBCO Films on Silicon 41

5 TRANSMITTANCE AND REFLECTANCE 54

Measurements of a Si Substrate 55
Measurements of the YBCO Films 56
Analysis of Transmittance and Reflectance of YBCO Films 59
Discussion 65

6 ABSORPTANCE OF YBCO FILMS 91

Results 92
Effect of the Film Thickness 93

page

Absorptance in the Superconducting State 95

7 FABRY-PEROT RESONATORS 103

Theoretical Background 103
Review of F-P Resonators Built with HTSC Thin Films 105
Experiments 107
Calculation and Comparison 109
Discussion 112

8 SUMMARY AND CONCLUSIONS 125

Radiative Properties of the YBCO Films 125
Fabry-Perot Resonators 127

APPENDIX 127

REFERENCES 127

BIOGRAPHICAL SKETCH 134

NOMENCLATURE

A = absorptance

A_l = amplitude of forward propagating beam in l^{th} layer, V m^{-1}

B_l = amplitude of backward propagating beam in l^{th} layer, V m^{-1}

c_0 = speed of light in vacuum, 2.9979×10^8 m/s

D = dynamical matrix

d = cavity length or thickness, m

d_{Si} = thickness of the Si substrate, cm

E = electric field vector, V m^{-1}

e = charge of an electron, 1.602×10^{-19} C

F = finesse

f_s = fraction of superconducting electrons

G = thermal conductance, W/K

I = intensity of the beam

i = $(-1)^{1/2}$

j = electric current density, A m^{-2}

j_c = critical current density of superconductor, A m^{-2}

k = wave vector, cm^{-1}

m = order of resonance

m_e = effective or rest mass of electron

N = complex refractive index

n = real part of the refractive index

n_e = number density of electrons, m^{-3}

P = propagation matrix

R = reflectance; or resistance, Ω

r = reflection coefficient

S = responsivity, V/W

T = transmittance

t = transmission coefficient

T_c = critical temperature, K

$\mathcal{T}$ = transmittance of the resonator

$\mathcal{T}_{\text{res}}$ = resonant transmittance

u = moving mirror velocity m $\sec^{-1}$

v = velocity of electron, m $\sec^{-1}$

x = retardation, m

y = dimensionless admittance of the film

β = phase shift inside the cavity, rad

γ_e = damping constant in the Lorentz term, rad/s; (1 rad/s = 5.3089×10^{-12} cm^{-1})

δ = phase change

ε = dielectric function

ε_0 = electric permittivity of free space, 8.8542×10^{-12} $\text{C}\cdot\text{V}^{-1}\cdot\text{m}^{-1}$

ε_∞ = high-frequency dielectric constant

θ = angle of incidence

κ = imaginary part of refractive index

λ = wavelength in vacuum, m

ν = frequency Eq. (4.1)

σ_{dc} = dc conductivity, $(\Omega\cdot m)^{-1}$

$1/\tau$ = electron scattering rate, rad/s

ϕ_m = phase shift upon reflection at surface m, rad

ψ = $\beta + \phi_m + \phi_n$, Eq. (3.41)

ω = frequency, cm^{-1} ($1\ cm^{-1} = 2.9979 \times 10^{10}$ Hz)

ω_e = center frequency, rad/s

ω_m = resonance frequency, cm^{-1}

ω_p = plasma frequency, rad/s

ω_{pe} = plasma frequency in the Lorentz term, rad/s

$\Delta\omega$ = free spectral range, cm^{-1}

$\delta\omega$ = spectral resolution, cm^{-1}

Subscripts

f = film or film side incidence

s = substrate or substrate side incidence

Si = silicon

Abstract of Dissertation Presented to the Graduate School
of the University of Florida in Partial Fulfillment of the Requirements
for the Degree of Doctor of Philosophy

FAR-INFRARED RADIATIVE PROPETIES OF SUPERCONDUCTING YBCO FILMS DEPOSITED ON SILICON SUBSTRATES

By

Ravi Kumar Adimula

December 1999

Chair: Zhuomin Zhang
Major Department: Mechanical Engineering

This work describes the experimental studies on the radiative properties of superconducting thin films in the far-infrared region. The transmittance and reflectances of superconductive $YBa_2Cu_3O_{7-\delta}$ (YBCO) films deposited in Si substrates were measured in the wavelength region from 100 to 1000 μm at temperatures between 10 and 300 K. The effects of interference, optical resonance, and antireflection on the radiative properties of high-temperature superconducting (HTSC) films have been observed and quantitatively analyzed.

For the first time, the reflectance of the HTSC film-substrate composites for radiation incidence on the substrate side (Backside reflectance) has been measured. The backside reflectance increases significantly from the normal state to the superconducting state at certain wave lengths; this experimentally demonstrates the HTSC films can be used to build far-infrared intensity modulators. The absorptance of the film-substrate composite has been derived from the measured reflectance and transmittance and analyzed from the perspective of designing superconducting radiation detectors. The absorptance for radiation incidence on the substrate side is higher than that for the film side incidence. The complex refractive index of the YBCO films was determined from the measured transmittance using the Drude model in the normal state and a two-fluid model in the superconducting state.

The transmittance of the Fabry-Perot resonators built from the HTSC thin films was measured and analyzed. Measurements were carried out for two different sets of resonator structures. The effect of partial coherence on the measured transmittance is studied in detail and the need to improve the resolution of spectrometer is emphasized. The resonant transmittance is a complex function of the cavity length, substrate thickness and phase shift upon reflection. The resonant transmittance reaches its maximum for a particular value of the cavity length and substrate thickness. Detailed discussion on the resonant transmittance optimization is provided which helps in choosing the optimal combination of the substrate thickness and the cavity length and it also helps in designing far-infrared resonators of higher finesse.

CHAPTER I
INTRODUCTION

A perfect superconductor is a material that exhibits zero resistance and perfect diamagnetism when it is maintained at temperatures below the critical temperature T_c, under bias current less than the critical current and applied magnetic field less than the critical magnetic field. Perfect diamagnetism, the second characteristic property, means that a superconductor does not permit an externally applied magnetic field (which is less than the critical magnetic field) to penetrate into its interior. The discovery of high-temperature superconductors (HTSC) by Bednorz and Muller in 1986 and Wu et al. in 1987 has generated tremendous excitement in the public because of the fact that the superconductivity can now be achieved above liquid-nitrogen temperature and the new technological promises of these materials (Gao, 1992). More and more materials recently have been found to be superconducting at higher and higher temperatures (Poole et al., 1995).

Spectroscopy played an important role in understanding features like the structural anisotropy and the energy gap of the HTSC materials. Most of these studies were done on thick films and single crystals. Later, focus has shifted to developing newer applications of HTSC, which require that superconductors be in the thin-film form grown on compatible substrates. Since then substantial work has been done in the areas of deposition of HTSC thin films and the substrate selection. Initial spectroscopic studies showed that HTSC thin films tend to show strikingly different radiative properties in the far-infrared region.

This dissertation analyzes the measured radiative properties of $YBa_2Cu_3O_{7-\delta}$ (YBCO) thin films deposited on silicon (Si) substrate. Two important issues are considered. The first one is interference effects and associated resonance in the film-substrate composite. The reflectance of a YBCO film increases rapidly as its state is changed from the normal to the superconducting. This higher reflectance causes the resonance effect within the substrate that alters the interference features of the film–substrate composite. This resonance effect can be used in Fabry-Perot resonators. The second issue is regarding the radiative properties of the film-substrate composite for radiation incident on the substrate side (henceforth referred as the backside illumination). The reflectance and absorptance values of thin films differ significantly for backside illumination as compared to the case when radiation incident on the film side. The higher backside reflectance and absorptance will be useful in building intensity modulators and bolometers of high responsivity (Zhang, 1998).

HTSC thin films on a transparent substrate are superior candidates for resonators than the metallic mesh especially in the far-infrared region (Renk et al., 1990). Metallic meshes show absorption due to the ohmic losses. The absorptance within the metallic mesh limits the finesse of the observed spectra of the resonators. In the superconducting state, the HTSC thin films have no ohmic losses (i.e., no absorption) for frequencies up to the superconducting gap. The superconducting gap lies within the far-infrared region; hence, the resonator built with HTSC thin films should offer a higher finesse than metallic mesh. The Fabry-Perot resonators built from the YBCO films deposited on Si substrate are studied in detail. Measurements and the analysis are provided to help in optimizing the resonator characteristics.

The organization of this dissertation is as follows. Chapter 2 presents some applications of HTSC thin films and a review of work that has been done related to the substrate selection and experimental and theoretical studies on HTSC materials. Theoretical background for the understanding of the physical properties of HTSC materials and for computing the radiative properties of multilayers is presented in Chapter 3. Infrared experimental techniques and the film deposition methods are described in Chapter 4. Transmittance and reflectance measurements on Si substrates and the YBCO films along with the analysis are presented in Chapter 5. The reflectance and transmittance data recast in the form of absorptance are discussed in Chapter 6 for the design and optimization of infrared detectors. Measurements and the optimization calculation of the Fabry-Perot resonators are presented in Chapter 7. Finally, conclusions and recommended future work are given Chapter 8.

CHAPTER 2
APPLICATIONS OF HTSC FILMS AND PREVIOUS STUDIES

This chapter presents discussion on the application aspects of HTSC thin films and the spectroscopic studies carried out in this regard. Some applications require HTSC materials to be in the form of a thin film deposited on a suitable substrate. Extensive work has been conducted to study the temperature dependent radiative properties of HTSC films. The radiative properties of HTSC films change rapidly from the normal state to the superconducting state in the far-infrared region. This significant change in the radiative properties coupled with the ability to alter the state by applying critical current or critical magnetic field or by raising temperatures above T_c make HTSC films suitable candidates in designing thermo-optoelectronic devices such as far-infrared intensity (amplitude) modulators, radiation detectors, and optical resonators.

Some Potential Applications of HTSC Thin Films

Far-Infrared Modulators

Conventionally, far-infrared radiation is modulated by means of mechanical chopping. The speed at which radiation is modulated is limited by the rotational inertia of the chopper. Some applications like signal processing of the far-IR probe beams used for plasma diagnostics, characterization of far-IR detectors and modulation of far-IR gas laser need the radiation to be modulated at very great speeds (Grossman, 1989). The transmittance and reflectance of HTSC films change strikingly when state of the film changes from normal to superconducting, which can be achieved by reducing the temperature to below the critical temperature. The HTSC film in the superconducting state (by virtue of its temperature being less than T_c) can be switched to normal state by applying an electrical current greater than the critical current. The fast switching from superconducting to normal state allowed by this way help in modulating the far-infrared radiation at much greater speeds than the conventional chopping method.

The reflectance of HTSC thin films differs significantly for the backside illumination as compared to radiation incident on the film side (see Fig 2.1). This feature allowed by the backside illumination is greatly helpful in high contrast far-infrared modulators (Zhang et al., 1998). Most of the work is presented for the reflectance of HTSC films for radiation incident on the film side (Renk, 1992; Tanner and Timusk, 1992; Zhang et al., 1994). In order to confirm the features associated with the backside illumination, measurements of the reflectance of HTSC films for backside illumination are presented by Kumar et al. (1999c).

Bolometers

The heating effect of the absorbed radiation can set in a change in the resistance of the material. The devices classified as bolometer detectors use this change in the resistance to measure the incident radiation. Initially, bolometers were constructed of evaporated metal films, but these devices are noisy and less sensitive. Bolometers composed of semiconductor alloys have been used in modern infrared work.

Figure 2.2 depicts the resistance variation with the temperature for a typical superconductor. Near the transition temperature (critical temperature T_c) the resistance drops from a finite value to zero. Also shown in Fig. 2.2 is the temperature derivative of the resistance (dR/dT) which registers a rapid increase and decrease near T_c. This large change in the resistance for a small change in the temperature indicates that the superconductors when operated near T_c can be used as bolometer elements.

A schematic of a superconducting bolometer is shown in Fig. 2.3. Modulated radiation is incident on the superconducting film, causing the temperature of the film-substrate composite to vary relative to that of a temperature-stabilized heat sink (Zhang and Frenkel, 1994). A constant bias current is applied and voltmeter measures the voltage across the film. Ohms law gives the change of the voltage ΔV as

$$\Delta V = I \frac{dR}{dT} \Delta T \tag{2.1}$$

where I is the bias current and ΔT is the temperature difference between the film-substrate composite and the heat sink. The ratio of the output voltage to the incident power is defined as the responsivity, S, and it is expressed as

$$S = \frac{A\,I(dR/dT)}{G(1+\omega^2\tau^2)^{1/2}} \tag{2.2}$$

where A is the absorptance of the detector, G is the thermal conductance, ω is the modulating frequency, and τ is the thermal time constant of the detector (Rice et al., 1994). Near the transition temperature, superconductors show larger value of dR/dT compared to metals and semiconductors hence the superconductor bolometers offer higher responsivity. One of the earliest applications conceived for HTSC films was the transition edge-bolometer, which can be operated using liquid N_2 temperature. The HTSC bolometers are not only economical but also offer higher responsivity and sensitivity than the standard uncooled bolometers, thermopiles and pyroelectric detectors (Richards, 1994).

Design criterion such as larger responsivity and lower noise equivalent power requires the absorptance α to be maximum in the film-substrate composite. For an optimized thermal and optical design of HTSC bolometer, Si is an ideal substrate because of its high thermal conductivity and low specific heat. The higher far-infrared transparency of Si allows backside illumination, which results in higher absorptance in the film-substrate composite. Several workers demonstrated the HTSC bolometers and in the near future this idea is expected to be available for commercial purpose (Carr et al., 1990; Fenner et al., 1993; Mechin et al., 1997; and Rice et al., 1994).

Fabry-Perot Resonators

Observations in the far-infrared region play an important role in the fields of astrophysics, chemical analysis, and molecular spectroscopy. Far-infrared studies in astrophysics include the cooling lines of star forming regions, associated cold dust, and spectra of giant planets (Brodbeck et al., 1998). The pure rotational spectra of molecules and absorption bands in solids and liquids generally fall in the far-infrared region.

Most of these studies require precise measurement of the far-infrared radiation in a very narrow band; this can be achieved with the help of Fabry-Perot (F-P) resonators (Vaughan, 1988). F-P resonators can also be used as adaptable interferometers and in laser-line analysis (Komm et al., 1975; Vaughan, 1989). A simple F-P resonator consists of two reflecting mirrors facing each other separated by a medium that is usually air or vacuum or a gas which needs to be analyzed. The most commonly employed reflectors in the far-infrared region are metallic meshes (Renk and Genzel, 1962; Belland and Lecullier, 1980).

A simple Fabry-Perot resonator, shown in Fig. 2.4, uses two plane parallel mirrors coated with highly reflecting material on one side, to produce an interference pattern in which all the incoming beam intensity is concentrated at a few wave numbers. HTSC thin films on a transparent substrate are better candidates than the metallic mesh especially in the far-infrared region (Renk et al., 1990). Metallic meshes show absorption due to ohmic losses from the current induced into the wires at infrared frequencies. This absorptance within the metallic mesh limits the finesse of the observed spectra of the resonators.

In the superconducting state, the HTSC thin films have no ohmic losses (i.e., no absorption) for frequencies up to the superconducting gap. The superconducting gap lies within the far-infrared region; hence, the resonator built with HTSC thin films should offer a higher finesse compared to metallic mesh. Another advantage is the suppression of high-frequency radiation, as HTSC materials are more opaque to the higher frequency than the metallic-mesh. Pechen et al. (1992) and Renk et al. (1990) presented measurements on F-P resonators built from HTSC films. Kumar et al. (1999a) presented the transmittance of resonators along with the peak transmittance optimization calculations. These studies demonstrate the potential of HTSC films for building far-infrared resonators.

Infrared Studies on HTSC Films

In the above-mentioned discussion on applications it was emphasized that for the development of HTSC applications, the choice of the substrate material is an important issue. Substrates commonly used for growing HTSC films include MgO, $SrTiO_3$, $LaAlO_3$, yttria-stabilized zirconia (YSZ), and sapphire (Phillips, 1996). Several promising far-infrared applications of HTSC films, such as bolometers, modulators, and resonators, demand that the substrate be transparent in the spectral region of interest. Fenner et al. (1993) presented transmittance measurements for various substrates, $NdGaO_3$, $LaAlO_3$, MgO, YSZ, and Si, in the mid- and far-infrared regions. This study showed that the transmittance of Si is generally higher than that of the other substrates in the measured spectral region. (The transmittance of pure Si is slightly greater than 0.5 at wavelengths longer than 20 μm.) The higher transmittance of Si in a broad spectral region allows new optical designs such as backside-illuminated HTSC microbolometers (Rice et al., 1994). At present, Si substrates have received significant attention from the electronics industry due to the feasibility of lithographically patterning HTSC films and the potential integration of semiconductor and superconducting electronics (Phillips, 1996). High-quality YBCO films have been successfully grown on Si substrates using pulsed laser ablation (Fork et al., 1991; Mechin et al., 1996) but very few measurements have been done to determine the radiative properties of such films.

Berberich et al. (1993) measured the transmittance and reflectance of imperfect YBCO films deposited on Si substrates. These films were of poor quality because they were deposited on Si substrates without buffer layers, and the reflectance was measured only at room temperature. Karrai et al. (1992) studied the transmittance of YBCO thin films on Si substrates with and without a magnetic field. However, the substrates were intentionally wedged to avoid interference effects. Most of the reported radiative properties of HTSC superconductors were for opaque samples or thin films on thick substrates (Tanner and Timusk, 1992; Zhang et al., 1994). For transmittance measurements, the interference effects associated with the substrate were often neglected by either averaging over a free spectral range or using wedged substrates (Gao et al., 1991; Karrai et al., 1992; Zhang et al., 1992; Cunsolo et al., 1993). Knowledge of the radiative properties of thin YBCO films deposited on thin substrates is essential for designing optoelectronic devices including radiation modulators and Fabry-Perot resonators (Renk et al., 1990; Genzel et al., 1992; Malone et al., 1993; Zhang, 1998).

The transmittance and reflectance of thin films on transparent substrates typically oscillate periodically as the optical frequency changes, as a result of multiple reflections inside the substrate. This oscillation is particularly prevalent in the far infrared because the wavelength is comparable with the substrate thickness. Hadni et al. (1995) measured the far-infrared transmittance of several YBCO films deposited on MgO substrates. The interference features associated with the substrate were clearly seen in their study at frequency 10 to 40 cm^{-1}. Kumar et al. (1999c) measured the transmittance spectra and reflectance spectra of YBCO films deposited on Si substrates in the frequency region 10 to 100 cm^{-1}. This study presented the reflectance from both the film side and the substrate side, also the effect of the film thickness on observed interference fringes.

Considering that high absorptance in the YBCO film is a crucial requirement in the construction of radiation detectors, there is a need to determine the absorptance of thin films. Phelan et al. (1992) investigated the thickness-dependent absorptance of YBCO films deposited on MgO substrates. Their measurements are in the wavelength region from 10 μm to 50 μm (1000 cm^{-1} to 200 cm^{-1}) at room temperature. Miller et al. (1993) presented film side absorptance of very thick (above 400 nm) YBCO films deposited on MgO, $SrTiO_3$, and $LaAlO_3$ substrates in the frequency region 10 cm^{-1} to 700 cm^{-1}. They concluded that the film side absorptance increases smoothly with frequency in the measured region. Renk et al. (1991) presented the far-infrared and microwave absorptance of 400 nm thick YBCO films deposited on $SrTiO_3$ substrate and provided information on the intragap (i.e., below the superconducting gap) absorptance. Higher absorptance of the film-substrate composite occur when radiation is incident on the substrate side (backside illumination). Backside illumination requires that the substrate be transparent in the measured spectral region. Kumar et al. (1999b) presented absorptance of YBCO films on Si substrates in the normal state for radiation incident on the film side and the backside.

Accurate assessments of the potential of YBCO films in optoelectronic applications require the determination of the frequency-dependent radiative properties. Knowledge of the complex dielectric function of the YBCO film facilitates the computation of radiative properties in desired spectral regions (Phelan et al., 1991; 1992). Due to their complicated crystalline structures, the refractive index of the HTSC materials may vary significantly depending on the method of preparation, oxygen content, thickness, and microstructure (Choi et al., 1992; Renk, 1992; Tanner and Timusk, 1992; Flik et al., 1992).

In the normal state, a two-component model, consisting of a temperature-dependent free-carrier absorption term (the Drude term) and a temperature-independent mid-infrared term (the Lorentz term), is used for computing $\varepsilon(\omega)$. In the superconducting state, the conventional two-fluid model is used for computing $\varepsilon(\omega)$. In the two-fluid model, the free carriers (represented by the Drude term in the normal state) are assumed to be in two different states often referred to as superconducting electrons and normal electrons. The superconducting electrons are not scattered by sources and are responsible for conducting the resistanceless current.

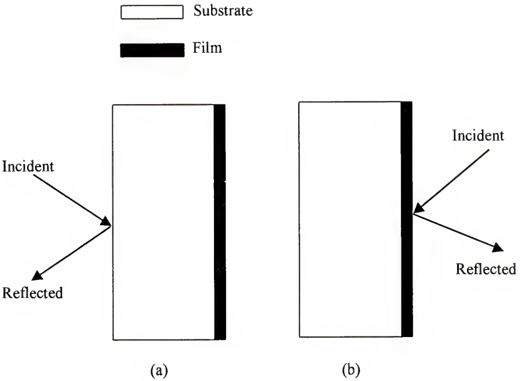

Figure 2.1. Configurations for (a) film side illumination (b) backside illumination

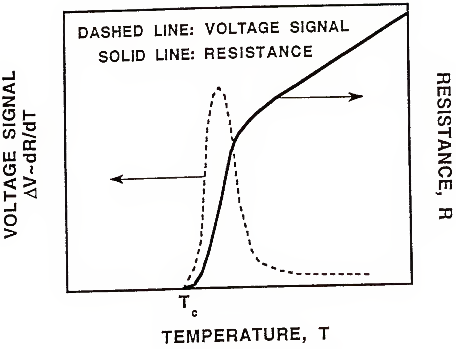

Figure 2.2 Temperature vs. resistance and dR/dT for a superconductor

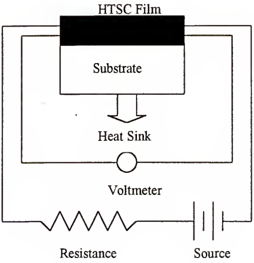

Figure 2.3 Schematic of a superconductor bolometer

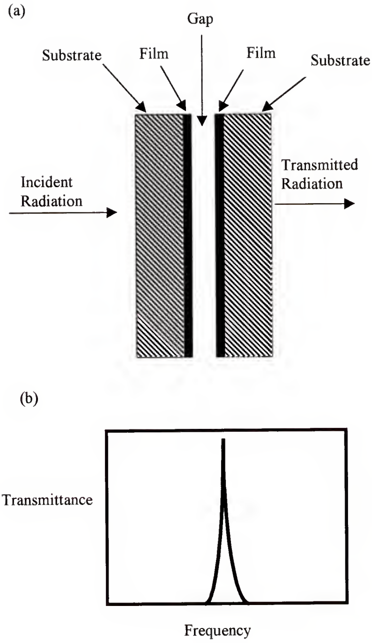

Figure 2.4 Construction and characteristics of Fabry-Perot resonator (a) schematic of a resonator (b) the transmitted radiation through the resonator vs. frequency

CHAPTER 3
THEORETICAL CONSIDERATIONS

The frequency dependent dielectric function $\varepsilon(\omega)$ and the electrical conductivity $\sigma(\omega)$ explain the radiation interaction at the atomic level and the associated absorptive and dispersive nature of the materials. However, neither $\varepsilon(\omega)$ nor $\sigma(\omega)$ can usually be measured directly. Therefore, the optical properties are usually determined from experimentally measured transmittance and/or reflectance, by assuming suitable models for the dielectric function.

Electrical Conductivity

D.C. Conductivity

In metals a background lattice of positive ions oscillating about the fixed lattice positions, are considered to be immersed in an electron gas made up of valence electrons. The negative charges on the mobile valence electrons exactly balances positive charges on the relatively immobile positive ions.

A potential difference between two points on a conductor establishes a uniform electric field, E, along the axis of the wire. This field accelerates the electrons, giving rise to electric current. The product of the electron charge (e) and the electric field (E) gives the accelerating force acting on the electrons. The continuous movement of electrons will result in repeated collision with the stationary atoms in the lattice. The collisions with the stationary atoms result in a damping force on the free electrons, which is proportional to the velocity. Thus the equation of motion for a single electron is

$$m_e\left(\frac{dv}{dt}\right)+\frac{m_e v}{\tau}=-eE \tag{3.1}$$

where m_e and v is the mass and the velocity of the electron respectively and t is the time. $1/\tau$ denotes the strength of damping and can also be interpreted as scattering rate of electrons. Solving Eq. (3.1) for the steady state velocity (i.e., $dv/dt=0$) of electrons

$$v=-\left(\frac{eE}{m_e}\right)\tau \tag{3.2}$$

The current density J is defined as

$$J=-n_e ev \tag{3.3}$$

Where n_e is the number density of electrons. Substituting Eq. (3.2) in to Eq. (3.3)

$$J=\left(\frac{n_e e^2 \tau}{m_e}\right)E \tag{3.4}$$

The DC conductivity σ_{dc} is defined by Ohm's law as

$$J=\sigma_{dc} E \tag{3.5}$$

Using Eq. (3.4) and Eq. (3.5) σ_{dc} is given as

$$\sigma_{dc}=\frac{n_e e^2 \tau}{m_e} \tag{3.6}$$

The scattering rate ($1/\tau$) is a basic parameter that determines the thermal and electrical transport properties and optical behavior of the materials. It is a measure of the resistance encountered by electrons as they move in the presence of the electric field. The scattering rate is determined by the probability of collisions between electrons and phonons, impurities,other electrons, and lattice defects. At high temperatures electron scattering due to phonons is the dominant process. At low temperatures, electron scattering is mainly caused by the presence of impurities or lattice imperfections. Similar temperature dependency is also expected for the resistivity ($1/\sigma_{dc}$) as it is directly proportionate to the scattering rate.

Frequency Dependent Electrical Conductivity

Instead of a stationary dc field, if a harmonically varying electric field of $E=E_0 e^{-i\omega t}$ where frequency ω, acts on the conductor, free electrons are accelerated periodically in the backward and forward directions as E reverses its sign on every cycle. This effect may be taken into force balance equation (3.1) by substituting $E=E_0 e^{-i\omega t}$

$$m_e \frac{dv}{dt}+\frac{m_e v}{\tau}=-eE_0 e^{-i\omega t} \tag{3.7}$$

Assuming the harmonically varying velocity of electrons v as $v=v_0 e^{-i\omega t}$ and solving for velocity v_0

$$v_0=\frac{-eE}{m_e}\frac{\tau}{1-i\omega\tau} \tag{3.8}$$

Using this expression for velocity in Eq (3.3) and subsequently solving for conductivity results in frequency dependent conductivity as

$$\sigma(\omega)=\frac{\sigma_{dc}}{1-i\omega\tau} \tag{3.9}$$

When $\omega\tau \ll 1$ many collisions occur during each cycle of the E field, and the average electron motion follows the oscillations thus steady dc conductivity can be assumed. For $\omega\tau \gg 1$, E oscillates more rapidly than the collision frequency, the conductivity predominantly becomes imaginary, corresponding to a reactive impedance.

Dielectric Functions

Maxwell's equations together with the Ohm's law can be employed to study the electromagnetic wave propagation inside the conducting medium. The resultant wave equation for electric field and the wave vector are complex. Further, it can be proved that inside a conductor the frequency–dependent complex dielectric function $\varepsilon(\omega)$ is related to frequency dependent conductivity by

$$\varepsilon(\omega) = \varepsilon_\infty + \frac{i}{\varepsilon_0 \omega}\sigma(\omega) \tag{3.10}$$

The complex refractive index related to complex dielectric as $\varepsilon = (n + i\kappa)^2$; where n is the real part and κ is the imaginary part of the refractive index, usually referred as optical constants. These optical constants are experimentally determined by measuring the transmittance or the reflectance in the specified frequency range and fitting data by assuming suitable dielectric models. The nature of the radiation interaction with materials is strongly influenced by the type of electrons, their motion to the applied electric field and the frequency of the radiation.

Optical properties of superconductors change rapidly from the normal state to the superconducting state. In the normal state dielectric function is dominated by the free electrons (Drude term) in the far-infrared region and by bound electrons (Lorentz term) in the mid-infrared region. The dielectric function in the superconducting state is dominated by the presence of the superconducting electrons also known as Cooper pairs that do not scattered by any sources. Thus, the dielectric function in the superconducting state is modeled by two-fluid model, which assumes that both the normal and superconducting electrons dominate the optical characteristic of the superconductor.

Normal State

In the normal state, the frequency-dependent complex dielectric function can be modeled as a sum of the Drude term ($\varepsilon_{\mathrm{Drude}}$), the Lorentz term ($\varepsilon_{\mathrm{Lorentz}}$), and a high-frequency constant ($\varepsilon_\infty \approx 5$):

$$\varepsilon(\omega) = \varepsilon_{\mathrm{Drude}} + \varepsilon_{\mathrm{Lorentz}} + \varepsilon_\infty \tag{3.11}$$

The Drude term describes the electronic behavior in the infrared region by assuming that free electrons are accelerated in the presence of an electric field and that collisions result in a damping force. Thus, the Drude term can be expressed as

$$\varepsilon_{\mathrm{Drude}} = -\frac{\omega_p^2}{\omega(\omega + i/\tau)} \tag{3.12}$$

where ω is the angular frequency, ω_P is the plasma frequency, and $1/\tau$ is the electron scattering rate. The plasma frequency is defined as $\omega_p^2 = n_e e^2 / m_e \varepsilon_0$, where n_e, e, and m_e are the electron number density, charge, and effective mass, and ε_0 is the electric permittivity of free space. The plasma frequency, the scattering rate, and the dc electrical conductivity σ_{dc} are related by

$$\omega_p^2 = \frac{\sigma_{dc}}{\varepsilon_0 \tau} \tag{3.13}$$

From Eqs. (3.12) and (3.13), only σ_{dc} and $1/\tau$ are needed to calculate the frequency dependent $\varepsilon_{\mathrm{Drude}}$.

The Lorentz term can be derived by assuming that the electrons are bound to their nuclei by harmonic forces and are subjected to damping forces. Lorentz terms are also commonly used to model infrared active phonons. The phonon contributions, however, can be neglected compared to the electronic contributions (Choi et al., 1992). This neglect is particularly valid in the far infrared because the resonant frequencies of most phonons are in the mid-infrared region. For HTSC materials, however, there is a broadband mid-infrared electronic absorption, which is typically modeled with a Lorentz term (Tanner and Timusk, 1992). This contribution is therefore expressed as

$$\varepsilon_{\text{Lorentz}} = \frac{\omega_{pe}^2}{\omega_e^2 - \omega^2 - i\omega\gamma_e} \tag{3.14}$$

where ω_{pe}, ω_e and γ_e are respectively the plasma frequency, center frequency and damping constant of the mid–infrared band.

Superconducting State

Many properties of the superconductors can be explained in terms of a two-fluid model that postulates that in the superconductor a fluid of normal electrons coexists with a superconducting electron fluid. These two fluids interpenetrate but do not interact. According to the two-fluid model, interaction between a pair of electrons and a phonon near the neighborhood of an ion lead to formation of a electron pair also known as a Cooper pairs. These Cooper pairs can be treated as a single boson particle which obey Bose-Einstein statistics but do not obey the Pauli exclusion principle, which allow Cooper pairs to occupy the same state. The bound pair of electrons occupy the same state, overlap with each other because the distance between pairs is much less than the large size of pair. This extremely high degree of overlap among pairs is such that densely associated pairs can not show independent motion; they are capable of only collective motion (Goldman and Markovic, 1998). Because of the density of Cooper pairs is very high, only a correspondingly small velocity is required for them to generate a considerable current (see Eq 3.3). This explains the high current densities carried by the superconductors.

Other important characteristic of Cooper pairs is their high de Broglie wavelength $\lambda = h/mv$, because the velocity of Cooper pairs is very small, now λ has macroscopic dimension. This single de Brogli wavelength describes all of the Cooper pairs because all of them have same set of dynamic properties. This very large de Broglie wave is basically responsible for the ineffectiveness of the scattering. In general a wave can be scattered only when its wavelength is about the same as or smaller than the scattering source. The very long de Brogli wave is much larger than scattering sites such as impurities and most lattice imperfections that affect normal electrons. This explains the absence of scattering of Cooper pairs and persistence of the resistanceless current (Pollack, 1990).

In the superconducting state only a fraction of available electrons (f_s) are assumed to be in the condensed phase (or superconducting state) and the remaining electrons are in the normal state. As mentioned above, the superconducting electrons move without any scattering, and the value of f_s assumed to be temperature dependent. The contribution of the superconducting electrons to the dielectric function is

$$\varepsilon_{\sup} = -\frac{\omega_p^2}{\omega^2} + i\pi\delta(\omega)\frac{\omega_p^2}{\omega} \tag{3.15}$$

The Drude term remains due to the presence of normal electrons with a number density of $(1-f_s)n_e$. The dielectric function in the superconducting state is therefore modeled as

$$\varepsilon(\omega) = f_s\varepsilon_{sup} + (1-f_s)\varepsilon_{Drude} + \varepsilon_{Lorentz} + \varepsilon_{\infty} \tag{3.16}$$

Radiative Properties of Multilayers

The radiative properties of multilayers can be calculated from the prior knowledge of their refractive index of the materials and their thickness. For the number of layers more than two, the matrix method is convenient to obtain the resultant radiative properties of the multilayer structure. This method is often requires computer to handle the matrix algebra. The expressions for reflectance, transmittance and absorptance can also be derived by summing the amplitudes of successive reflections and refractions. This method of amplitude summation is referred to as Airy's formulas, and is generally used for freestanding films or for two layer structures. In the following sections, the matrix method and Airy's formulas are presented in detail.

Matrix Method

The radiative properties of materials can be calculated from the prior knowledge of their complex refractive indices. Usually the HTSC thin films are deposited on a substrate. In order to avoid any lattice disorientation and reaction between YBCO and Si, buffer layers are placed between the film and the Si substrate. They are in the form of thin layers adjacent to each other. The transfer matrix method is a convenient approach for calculating the radiative properties of such layered structures. In this method, each layer is assumed homogeneous and isotropic. Further assumption is made that the radiation is essentially coherent inside the films. The boundary conditions for the electric and magnetic fields are that the tangential component of the electric field and the normal component of the magnetic field are continuous across each interface (Zhang and Flik 1993).

For a layered structure, as shown in Fig. 3.1, regions 1 and N+1 are semi-infinite media and there are N−1 layers and N interfaces. In Fig. 3.1, A_l and B_l are the amplitudes of the forward and backward propagating plane waves at the interface and n_l is the complex refractive index of the l^{th} layer. From the general solution of plane-wave equations, the electric field distribution can be written as

$$E(x) = A_l e^{ik_l(x-x_l)} + B_l e^{-ik_l(x-x_l)} \qquad l = 1,2,\ldots,N+1 \qquad (3.17)$$

where X_{N+1} is set equal to X_N since there are only N interfaces and $k_l = (n_l\omega/c_0)\cos\theta_l$ is the wave vector, c_0 is the speed of light in vacuum, and θ_l is the (complex) angle of propagation. By applying the boundary conditions, the electric field amplitudes are related by

$$\begin{bmatrix} A_l \\ B_l \end{bmatrix} = D_l^{-1} D_{l+1} P_{l+1} \begin{bmatrix} A_{l+1} \\ B_{l+1} \end{bmatrix}, \quad l = 1,2,\ldots,N \qquad (3.18)$$

where the dynamical matrix D_l is given as

$$D_l = \begin{bmatrix} 1 & 1 \\ n_l\cos(\theta_l) & -n_l\cos(\theta_l) \end{bmatrix}, \text{ for s wave}$$

$$D_l = \begin{bmatrix} \cos(\theta_l) & \cos(\theta_l) \\ n_l & -n_l \end{bmatrix}, \text{ for p wave} \qquad (3.19)$$

and D_l^{-1} is the inverse of D_l. The propagation matrix P_l is given as

$$\mathrm{P}_l = \begin{bmatrix} e^{-ik_l(x_l - x_{l-1})} & 0 \\ 0 & e^{\,ik_l(x_l - x_{l-1})} \end{bmatrix} \tag{3.20}$$

Equation (3.18) can be rewritten as

$$\begin{bmatrix} \mathrm{A_j} \\ \mathrm{B_j} \end{bmatrix} = \begin{bmatrix} \mathrm{M}_{11}^{\mathrm{j}} & \mathrm{M}_{12}^{\mathrm{j}} \\ \mathrm{M}_{21}^{\mathrm{j}} & \mathrm{M}_{22}^{\mathrm{j}} \end{bmatrix} \begin{bmatrix} \mathrm{A_{N+1}} \\ \mathrm{B_{N+1}} \end{bmatrix}, \ \mathrm{j} = 1, 2, \ldots, \mathrm{N} \tag{3.21}$$

where

$$\begin{bmatrix} \mathrm{M}_{11}^{\mathrm{j}} & \mathrm{M}_{12}^{\mathrm{j}} \\ \mathrm{M}_{21}^{\mathrm{j}} & \mathrm{M}_{22}^{\mathrm{j}} \end{bmatrix} = \prod_{l=j}^{N} \mathrm{D}_l^{-1} \mathrm{D}_{l+1} \mathrm{P}_{l+1} \tag{3.22}$$

If the radiation is incident from medium 1, the electric field reflection and transmission coefficients are given as

$$\mathrm{r} = \frac{\mathrm{B_1}}{\mathrm{A_1}} = \frac{\mathrm{M}_{21}^{1}}{\mathrm{M}_{11}^{1}} \tag{3.23}$$

$$\mathrm{t} = \frac{\mathrm{A_{N+1}}}{\mathrm{A_1}} = \frac{1}{\mathrm{M}_{11}^{1}} \tag{3.24}$$

The power reflectance and transmittance are

$$\mathrm{R} = \left| \frac{\mathrm{M}_{21}^{1}}{\mathrm{M}_{11}^{1}} \right|^2 \quad \text{and} \quad \mathrm{T} = \left| \frac{1}{\mathrm{M}_{11}^{1}} \right|^2 \tag{3.25}$$

In Eq. (3.25), it is assumed that $n_{N+1} = n_1$. Finally, the absorptance, A, is calculated from the energy balance as

$$\mathrm{A} = 1 - \mathrm{R} - \mathrm{T} \tag{3.26}$$

Airy's Formulae

In this method, an unit intensity is assumed incident on a thin film structure, part of it is reflected and part of it is transmitted. By tracing the reflected and refracted energy, the total reflected energy (reflectance), transmitted energy (transmittance) and absorbed energy (absorptance) can be calculated. This method often referred to as ray-tracing method (Siegel and Howell, 1992).

Consider a beam is incident from the left (see Fig. 3.2). The incident beam is partially reflected and partially transmitted at the interface. The transmitted part is subsequently reflected back and forth between the two interfaces as shown. The reflection and transmitted coefficients can be obtained by adding the amplitudes of the successive reflected and transmitted rays. Taking the phase difference $\delta = 2\pi N d/\lambda$ introduced by the thickness of the film into account and adding the amplitudes of the reflected rays, we obtain the reflection coefficient (r)

$$r = r_{12} + t_{12}\, t_{21}\, r_{23} \exp(2i\delta) + t_{12}\, t_{21}\, r_{23}\, r_{21}\, r_{23} \exp(2i\delta) + \ldots\ldots$$

$$= \frac{r_{12} + r_{23} \exp(2i\delta)}{1 + r_{12}\, r_{23} \exp(2i\delta)} \qquad (3.27)$$

where

$$r_{jk} = \frac{N_J - N_k}{N_j - N_k} \quad \text{and} \quad t_{jk} = 1 + r_{jk} \qquad (3.28)$$

are the complex Fresnel coefficients of reflection and transmission for normal incidence and $N_j = n_j + i\kappa_j$ is the complex refractive index of the *j*th medium. Also note that while deriving Eq. (3.27) the principle of reversibility $(t_{ij}\, t_{ji} - r_{ij}\, r_{ji} = 1)$ has been used. Similarly, the transmission coefficient (t) is obtained as

$$t = t_{12}\, t_{23} \exp(i\delta) \left[1 + r_{21}\, r_{23} \exp(2i\delta) + (r_{23}\, r_{21} \exp(2i\delta))^2 + \ldots\ldots \right]$$

$$= \frac{t_{12}\, t_{23} \exp(i\delta)}{1 + r_{12}\, r_{23} \exp(2i\delta)} \qquad (3.29)$$

The power reflectance and transmittance are obtained as

$$R = |r|^2 \qquad \text{and} \qquad T = \frac{N_3}{N_1}|t|^2 \tag{3.30}$$

Two-Layer Structure

The above discussion can be extended to a two-layered structure consisting of a thin film on a thin substrate. The simplified Airy's formulae for computing the reflectance and the transmittance can be derived by tracing the reflection and transmission amplitudes at each interface. Let d_f and d_s be the thickness of the film and substrate, respectively and $N_j = n_j + i\kappa_j$ as the complex refractive index of air (j = 0), film (j = f) and substrate (j = s). The transmittance (T), reflectance form the film side (R_f) and the reflectance from the substrate side (R_s) are

$$R_f = \left|\frac{r_{of} + r_s \exp(i2\delta_f)}{1 - r_{fo} r_s \exp(i2\delta_f)}\right|^2 \tag{3.31}$$

$$R_s = \left|\frac{r_{os} + r_b \exp(i2\delta_s)}{1 - r_b r_{so} \exp(i2\delta_s)}\right|^2 \tag{3.32}$$

$$T = \left|\frac{t_a t_{so} \exp(i2\delta_s)}{1 - r_b r_{so} \exp(i2\delta_s)}\right|^2 \tag{3.33}$$

where

$$r_b = \left|\frac{r_{sf} + r_{fo} \exp(i2\delta_f)}{1 - r_{fo} r_{fs} \exp(i2\delta_f)}\right| \tag{3.34}$$

is the ratio of the transmitted to incident electric field at the substrate-film interface,

$$r_s = \left|\frac{r_{fs} + r_{so} \exp(i2\delta_s)}{1 - r_{sf} r_{so} \exp(i2\delta_s)}\right| \tag{3.35}$$

is the ratio of the reflected to incident electric field at film-substrate interference including and absorption effects in the substrate, and

$$t_a = \left| \frac{t_{of}\, t_{fs} \exp(i2\delta_f)}{1 - r_{fo} r_{fs} \exp(i2\delta_f)} \right| \qquad (3.36)$$

is the ratio of the transmitted to the incident electric field and $\delta_f = 2\pi N_f d_f / \lambda$ and $\delta_s = 2\pi N_s d_s / \lambda$ are the complex phase change in the film and the substrate respectively.

Admittance Method

Very thin metallic films deposited on dielectric substrates generally are used in electronic and optical industries. Spectroscopic studies on these films especially in the far-infrared region provide a means to obtain the dc conductivity of the films. Consider a thin metallic film of thickness $d_f << \lambda$, wavelength of the far-infrared radiation, deposited on a dielectric substrate of refractive index N_1, as shown on Fig. 3.3. The transmittance through, T_{12}, and reflectance from, R_{12}, at the interface for radiation incident on the substrate side can be approximated as (Gao et al., 1996)

$$T_{12} = \frac{4N_1}{|N_1 + 1 + y|^2} \qquad (3.37)$$

$$R_{12} = \left| \frac{N_1 - 1 - y}{N_1 + 1 + y} \right|^2 \qquad (3.38)$$

where y is the complex admittance of the metallic film. In the very far-infrared region, the sheet admittance (McKnight et al.,1987; Kumar et al., 1999c)

$$y \approx \sigma_{dc} d_f / c_0 \varepsilon_0 \qquad (3.39)$$

Hence, from the measured far-infrared reflectance or transmittance the value of dc conductivity σ_{dc} can be obtained. Equation (3.38) shows that if $y = N_1 - 1$ the interface is impedance matched and the power reflectance R_{12} will be zero. Since y is positive this can happen when $N_1 > N_2$, i.e., propagation from a dense more dense to a less dense optical media. A coating having a suitable admittance value will eliminate the back surface reflectivity and therefore, the interference fringes within the dielectric slab.

Two Effective Surface Interface Method

In practical design of multilayers it is useful to assess the contribution of one particular film this can be done by two effective interface method. Consider the multilayer arrangement shown in Fig. 3.4 with two adjacent surfaces M and N. All the surfaces to the left of M and including M may be considered as system 1 and represented by $r_1^+, r_1^-, t_1^+ \text{and}\ t_1^-$, similarly system 2 comprising surfaces to the right of N and including N, is represented by $r_2^+, r_2^-, t_2^+ \text{and}\ t_2^-$. The amplitude of the transmitted light is same as given by Eq (3.29)

$$t = \frac{t_1^+ \, t_2^- \, e^{i\psi}}{1 + r_1^- \, r_2^+ e^{2i\psi}} \tag{3.41}$$

In this expression $\psi = \phi_M + \phi_N$ where ϕ_M and ϕ_N are the phase change upon reflection at surfaces M and N (Vaughan, 1988). The corresponding transmitted intensity I_t is found from square modulus i.e.,

$$I_t = \frac{\left|t_1^+ t_2^+\right|^2}{1 + \left|r_1^- r_2^+\right|^2 - 2\left|r_1^- r_2^+\right| \cos\psi}$$

$$= \frac{T_1 T_2}{(1 + R_1 R_2 - 2\sqrt{R_1 R_2} \cos\psi)} \tag{3.42}$$

here T_1, T_2, R_1, and R_2 are the intensity reflection and transmission coefficients. The above expression provides a means to examine the effect of a single layer on the total transmittance of the multilayer structure. Similarly, the effect of the single layer can also be studied on the total reflectance of the structure through the expression

$$I_R = \frac{\sqrt{R_1 R_2}(2 - 2\cos\psi)}{1 + R_1 R_2 - 2\sqrt{R_1 R_2} \cos\psi} \tag{3.43}$$

The two-effective layer method helps in identifying the effect of a single layer on the total transmittance and reflectance of the multilayer structure.

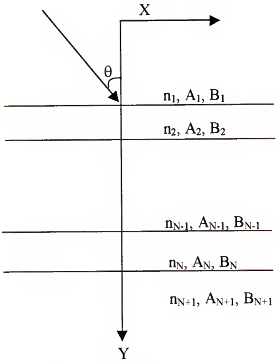

Figure 3.1 A multilayer structure

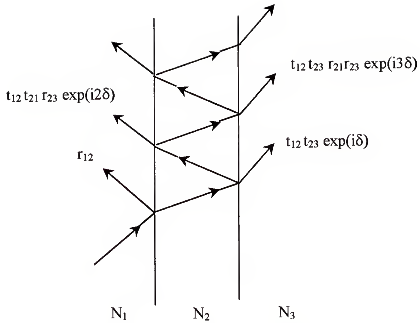
$t_{12}\,t_{23}\,r_{21}r_{23}\,\exp(i3\delta)$
$t_{12}\,t_{21}\,r_{23}\,\exp(i2\delta)$
$t_{12}\,t_{23}\,\exp(i\delta)$
r_{12}
N_1
N_2
N_3

Figure 3.2 Airy summation

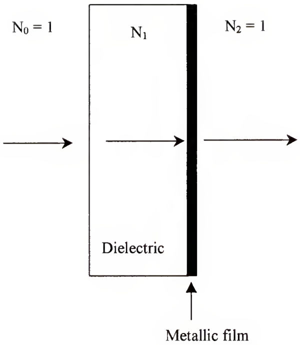

Figure 3.3 Thin metallic film on a dielectric substrate

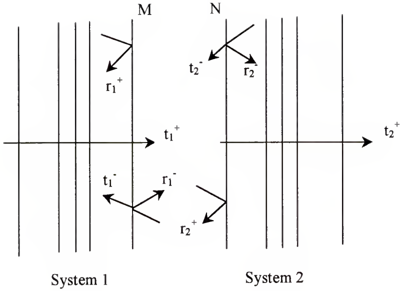

Figure 3.4 Representation of a multilayer system by two effective interfaces

CHAPTER 4
EXPERIMENTS

This chapter describes the spectroscopic equipment, measurement techniques and the YBCO film preparation method. The spectra were measured using the Michelson interferometer and the Bruker interferometer. An introductory theory on the interferometry and the details of the spectroscopic equipment used in the present study are described followed by the transmittance and reflectance measurement techniques. Sample films were prepared by the pulsed laser ablation method. The deposition process and the choice of the substrate play an important role for growing good quality films. In the second part of the chapter, the substrate requirements for growing a good quality film are emphasized. Later the laser ablation technique and the film preparation method are described.

Far-Infrared Measurements

The frequency of the radiation was measured in wave numbers (reciprocal of wavelength) through out this work. A typical infrared experiment used in this study is illustrated schematically in Fig 4.1. Radiation from the source passes to the modulator where its amplitude is modulated periodically in time. The frequency adopted for the modulation is as high as possible but not to be so high that the detector is unable to respond (Chantry, 1984). The modulated radiation is then passed into the radiation processor, which consists of interferometer and the sample film. The radiation, which has interacted with thesample film heads toward the bolometer detector. The detector signal further is amplified with the help of an amplifier. The lock–in device receiving the reference signals from the modulator will amplify only those detector signals that are in coherence with the reference signals. This procedure eliminates the background noise in the detector output signal. The output signal from the lock-in device is in analogue form, and is converted in to digital signal with the help of A/D converter and finally a personal computer is used to acquire this digital information.

Interferometry

The spectrometers used in this study are a slow–scan Michelson interferometer in the region 10 to 100 cm^{-1} and a Bruker Fourier transform interferometer (FT–IR) in the region 14 to 600 cm^{-1}. Interferometry that uses the entire radiation power at all frequencies is much superior than the grating spectrometer which uses only limited radiation available in the region of measurements. This is especially an important factor when measuring in the far-infrared region due to the fact that all thermal sources show energy starvation at low frequencies (which can be verified from the Plank law for spectral distribution of a black body radiation).

Interference between the two light beams coming from a single source, can be produced by introducing a path difference between these two beams. This mechanism is used by Michelson interferometer to produce an interferogram. Schematic representation of Michelson interferometer is shown in Fig. 4.2. A semi-reflecting beam splitter B divides radiation from the source S, into two parts of equal intensity. These two beams are reflected by a stationary mirror M_1 and a moving mirror M_2 and are then recombined to enter the detector D. The movement of the mirror M_2 introduces path difference between the two beams. If the mirror is moved at a constant velocity, the signal at the detector will be seen to vary sinusoidally, with a maximum is being registered each time when the path difference is a multiple integral of wavelength. Assuming the two beams have an equal intensity 0.5 I(ν), the intensity of the beam reaching detector is (Griffiths and de Haseth, 1986)

$$I(x) = 0.5 I(\nu) \left[1+\cos(2\pi\nu x)\right] \tag{4.1}$$

Here $x = 2ut$ is the retardation that equals to the path difference between the beams travelling to and from the mirror, u the mirror velocity and t the time. I(x) called as the interferogram, contains the information about frequency and path difference. For a polychromatic source emitting a continuous spectrum from $\omega = 0$ to $\omega = \infty$ above equation must be integrated to obtain the total intensity given as

$$I(x) = \int_0^\infty 0.5 I(\nu)\, d\nu + \int_0^\infty 0.5 I(\nu) \cos(2\pi\nu x)\, d\omega \tag{4.2}$$

It can be observed that interferogram I(x) is composed of a constant (dc) component and a modulated (ac) component correspond to the first term and the second term in Eq. 4.2. The dc component is nothing but a constant that equal to half of the total intensity emitted from the source (can be verified by making x = 0). Thus the Eq. 4.2 is reduced to

$$I(x) = \text{const} + \int_0^\infty 0.5 I(\nu) \cos(2\pi\nu x)\, d\nu \tag{4.3}$$

in Equation. 4.3, it can be said that I(ν) is a cosine Fourier transform of I(x) therefore the spectrum I(ν) can calculated by computing the inverse Fourier transform of I(x) given as

$$I(\nu) = 2\int_0^\infty I(x) \cos(2\pi\nu x)\, dx \tag{4.4}$$

In practice, the obtained interferogram (Eq. 4.3) may need to be modified by taking into account of the beam splitter efficiency, detector response and the amplifier characteristics.

The Bruker Interferometer

Reflectance was measured using an IBM-Bruker fast-scan spectrometer. The frequency covered was in the range of 14 to 600 cm^{-1}. As illustrated in Fig.4.3., the system is divided into four chambers: source, interferometer, sample and detector. A Hg arc lamp is used for measured far-infrared purpose. The sample chamber consists of two identical channels which can used for reflectance and transmittance measurements. For reflectance measurements, the optical stage shown in top part of Fig.4.3., is placed into the chamber. The entire system is evacuated to avoid H_2O and CO_2 absorption during measurements. Light for the source is focused onto the beam splitter and is then divided into two components one reflected and other transmitted. Each beam is imaged onto the faces of a movable two-sided mirror. These two beams retrace their route back to the beam splitter for recombination. The recombined beam is sent into the sample chamber and then into the detector. Because of the two-sided mirror the path difference $x = 4\,u\,t$ is introduced, where t is the time since the mirror is at the zero-path difference position, u is the mirror velocity. The optical frequency ν that is reaching the detector is amplified by a wide-band audio amplifier and then digitized by a 16-bit analog to digital converter. The digital acquired by the computer is Fourier transformed into a single-beam spectrum after necessary corrections such as apodization and phase corrections.

The Slow-scan Michelson Interferometer

Transmittance was measured with a slow scan Michelson interferometer. In comparison with the Bruker, it has a better signal to noise ratio at low frequencies due to larger and brighter mercury source. As shown in Fig.4.4 the light is modulated by a rotating aluminum chopper. In order to allow lock-in detection, the chopper also modulates the light falling on a photodiode from a small LED and the photodiode output serves as the reference signal. A mylar beam splitter in combination with optical filters was used to measure the spectra in range from 10 to 100 cm^{-1}. The movable mirror is mounted on a 20-cm comparator screw that permits in principle a resolution of 0.025 cm^{-1}. The screw is driven by a stepping motor and the step size determines the resolution. The stepping motor activated by a preset indexer that may be set to advance the stepping motor the appropriate number of steps whenever it receives the triggering signal. In order to avoid the absorption by the atmospheric gases the entire interferometer system was evacuated during the measurements.

Bolometer

For operation in the far infrared where photon energies are very low a detector of high sensitivity and signal-to-noise ratio is needed to measure the signal. One kind of detector with adequate sensitivity is He-cooled bolometer. The heating effect of absorbed radiation causes change in the resistance of the detector element at low temperatures. This change in resistance is calibrated in terms of incident radiation. The bolometer used in this work employs Si as the detector element. The bolometer system consists three main parts: detector element, liquid helium dewar, and preamplifier. Figure 4.5 illustrates a sketch of bolometer. A thermal radiation shield is placed helium can and case to reduce the heat load on the cold area. The optical signal is guided by an optical pipe through a polythene window and optical filters before it arrives at the detector element. The output signal is amplified and then further processed.

Transmittance and Reflectance Measurements

The transmittance and reflectance of films were measured at temperatures 10, 50, 100, and 200, and 300 K. The cooling system consists of cryostat, transfer line and helium supply dewar. Figure 4.6 shows the liquid–He flow diagram during the experiments. The sample film temperature can be varied with the controlled flow of liquid helium in combination of an external heater. The sample holder used for the transmittance measurements is shown in Fig. 4.7. Two identical copper plates with equally sized apertures (≈6 mm in diameter) were mounted at a right angle on the sample holder; One aperture is covered by the specimen and the other is left blank for the reference measurement. As shown in the Fig. 4.7. slightly curved beryllium copper strips (2 mm wide, 0.2 mm thick, and 5 mm long), fastened with screw on the corners of one plate, acted like springs (due to their high elasticity) to hold the film to the copper plate.

Schematic of the cryostat is shown in Fig. 4.6. It has an exhaust gas heater, exhaust gas port, vacuum pump out port, second cold stage to which the radiation shield is attached and the first cold stage (the cold finger). The sample holder is mounted on the cold finger of the cryostat. The cold finger is kept in high vacuum and cooled by flowing liquid He at 4.2 K, which results in conductive cooling of the specimen. A diffusion pump is used in order to achieve a vacuum of 10^{-2} Pa inside the cryostat before cooling;

the actual pressure should be much lower due to cryopumping. The specimen temperature was measured using a Si diode. An automatic temperature controller was used to adjust the temperature of the specimen using a proportional-integral-derivative (PID) control scheme and an electric heater wrapped around the cold finger. The temperature variation was within 0.5 K of the set temperature for measurements above 100 K. During the measurements at 10 K and 50 K, the variation of temperature was about 1 K from the set temperature.

The cryostat, along with the sample holder, is introduced vertically into the interferometer chamber. The cryostat can be rotated so that either the blank aperture or the specimen is in the beam path of the far-infrared radiation. For the transmittance measurement, the spectrum obtained with the blank is taken as the background spectrum. The cryostat is then rotated by 90° to introduce the specimen in the beam path. The exact position of the cryostat for the blank aperture or for the specimen is determined by gently rotating the cryostat until the signal is maximum. The transmitted spectrum of the specimen is divided by the background spectrum to obtain the transmittance. The spectral resolution is approximately 0.5 cm^{-1}.

The reflectance was measured using Bruker Fourier transform spectrometer. The spectrum is averaged over 128 scans and the resolution is $\approx 1\ \text{cm}^{-1}$. A schematic of reflectance measurement arrangement is shown in Fig. 4.8. Here, the far-infrared beam is directed to either the specimen or a Au mirror by a combination of plane and elliptical mirrors. The angle of incidence in the reflectance measurement is $\approx 7.5°$ with a beam divergence of 7.5°. The Au mirror is used as the reference for the reflectance measurements at all temperatures. In the far-infrared region, the reflectance of the gold is greater than 0.995 at room temperature and increases at lower temperatures. Hence, the reflectivity of the Au mirror is taken to be 1. During experiments sometimes it was observed that the optical alignment suffers after insertion of heavy transfer tube. All the room temperature measurements with transfer tube and without the transfer tube, in the cryostat, were compared. This provided a means to examine the alignment.

YBCO Films on Silicon

Among all the high temperature superconducting materials, YBCO has received most of the attention. Initially, YBCO films with high values of critical temperature (T_c), narrow transition widths and very high values of critical current density (J_c) have been made only on a few single crystal substrates. YBCO films having T_c equal to 90 K and J_c exceeding 10^6 A cm^{-2} have been made on single crystal substrates of MgO and $SrTiO_3$ by various techniques such as coevaporation, sputtering, chemical vapor deposition and laser ablation method (Mogro-Campero, 1989). However, there is a need to produce high quality films on Si, the primary material for electronics. Silicon is cheap, available and integrable substrate and nonabsorbing in the infrared region thus making it an ideal substrate for some of the conceived infrared applications of HTSC films.

The HTSC materials have complex crystalline structure. A schematic of the YBCO crystal structure is shown in Fig. 4.9. The O_2 content in the YBCO is very critical parameter while determining the properties of the film as it determines the free carriers in the YBCO material. Choi et al. (1992) presented the radiative properties of the $YBa_2Cu_3O_{7-\delta}$ films with varying O_2 content. The material with high O_2 content ($\delta = 0$) has metallic optical behavior and the one with low O_2 content ($\delta = 1$) has dielectric behavior. Many researchers investigated this feature and concluded that for obtaining high critical temperatures (i.e., the optimum doping) δ should be between 0.2 to 0.6 (Choi et al., 1992). The YBCO films need to be preserved in vacuum as any exposure to the atmosphere may alter the O_2 content and subsequently the material may loose its superconducting characteristics.

Also shown in the Fig. 4.9 are the coordinates of the crystalline structure. The HTSC materials are anisotropic in nature with J_c much higher in the direction perpendicular to the c-axis of the crystal (i.e., in the a-b plane) than along the c-axis. This anisotropy explains that in order make films with the highest values of J_c they should have c-axis aligned perpendicular to the plane of the substrate. Thus, for the highest values of J_c, highly aligned or epitaxial films are desired. Such films have been made on single crystal MgO and $SrTiO_3$. Same results are also obtained on Si using epitaxial buffer layers (Aguiar et al., 1994).

The main problem with using Si as substrate is the chemical interaction and interdiffusion between the film and the substrate, which occurs during the annealing. Attempts to grow high quality YBCO films on a bare Si substrate have met with little success because of the surface oxide formation on Si that prevents epitaxial growth of the film. To minimize this film/substrate interaction one alternative is to place epitaxial buffer layers in between the film and the substrate. Other alternatives include growing very thick films that enables to move away from the interface region and to minimize the time required for thermal treatment process by developing a rapid thermal annealing technique.

Film Preparation

In the current work, laser ablation method was used for the sample films deposition. In a laser ablation system, the raw material required for the film deposition is hold in a target and there are multi targets with a provision to rotate the target holder. This enables one to make films of multicomponent materials. During the film deposition process, a high-power laser hits the target material and evaporates it forming a plume of evaporated material. The plume travels toward the substrate and deposited on to it. The whole process takes place inside a chamber with a controlled O_2 atmosphere, and with a window for the laser pulse from an external source (Boyce et al., 1989).

Sample films were prepared at National Institute of Standards and Technology (NIST) facility. The YBCO films were deposited by pulsed laser ablation using an excimer laser operated at a wavelength of 248 nm. A single–crystal (100) Si wafer, polished on both sides with a thickness of approximately 200 μm and a diameter of 76 mm, was used as the substrate. The wafer is slightly boron-doped and has an electric resistivity of $\approx$1000 Ω-cm. The Si wafer was cut into approximately 12 x 12 mm^2 pieces for the deposition of the YBCO. Ag paste was used to mount the substrate onto a substrate holder in the deposition chamber. At high temperatures, Ag may diffuse into the Si substrate. Therefore, a 320 nm thick SiO_2 layer was deposited by chemical vapor deposition (CVD) on the backside of the Si substrate before the application of the Ag paste. The substrate was heated to 1063 K for the deposition of a 20 nm thick YSZ layer and then a 10 nm thick CeO_2 layer on the Si substrate. A YBCO film of 35 nm was deposited on the top of the buffer layers at 1043 K in an optimized O_2 environment (Rice et al., 1994). The thicknesses of the thin films were determined by calibrations of the rate of deposition. The YBCO films formed this way are *a-b* plane oriented (*c*-axis is parallel to the surface normal) with a critical temperature (T_c) between 86 and 88 K.

Several steps are followed to remove the Ag paste and the SiO_2 layer. First, the YBCO film was covered by a photoresist. Second, nitric acid (HNO_3) was used to remove Ag paste and then hydrofluoric acid (HF) was used to etch off the SiO_2 layer. Third, the photoresist was removed using acetone. Finally, the film is rinsed with isopropanol. The structure of the film is shown in Fig. 4.10. Some damage to the film may have taken place during this stripping process since the critical temperature of several films dropped to 80 to 82 K after the removal of the photoresist. However, scanning electron microscopic (SEM) images showed no evidence for microcracks or other surface damage.

The precise control over the uniform film thickness is much needed especially when the film is used for optical studies. At the NIST facility, it was observed that film thickness vary by $\pm$ 20 nm over 1 cm for a film of 200 nm thickness. This corresponds to a 10 percent variation in the film thickness. The thickness variation is determined by patterning, etching and profilometer measurement. During the deposition process the shape of the plume that is reaching the substrate is not uniform. The film thickness distribution falls off toward the edges in approximately gaussian distribution due to the variations in the plume shape. The geometry of the plume center region is used for the film growth calculations. During the spectroscopic measurements on the films of area 12 x 12 mm^2, only the central most area equivalent to a 6-mm dia circle is exposed to the probing infrared beam. This ensures that the effect of the film thickness variation to be minimum on the obtained transmittance and reflectance.

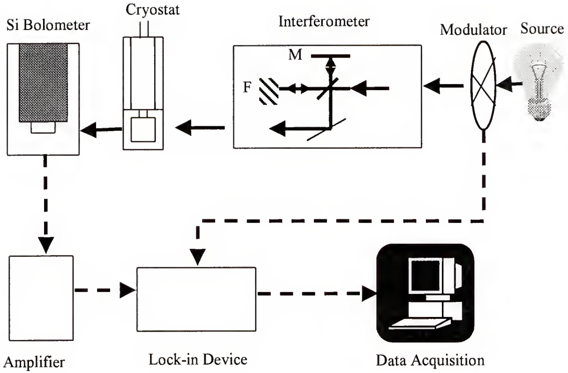

Figure 4.1 Experimental arrangement for infrared measurements

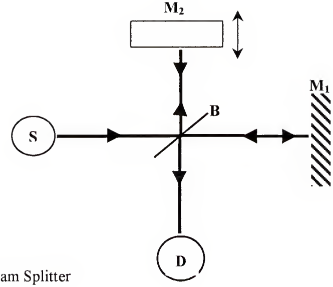

B Beam Splitter

D Detector

M_1 Fixed Mirror

M_2 Moving Mirror

S Source

Figure 4.2. Schematic diagram of Michelson interferometer

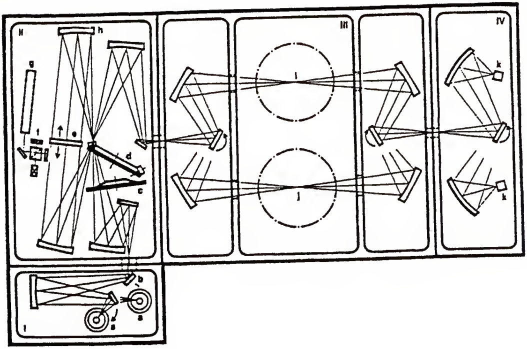

I **Source Chamber**
a Near, Mid, or far-IR sources
b Automated Aperture

II **Interferometer Chamber**
c Optical Filter
d Automatic Beam-splitter Changer
e Two-sided Movable Mirror
f Control Interferometer
g Reference Laser
h Remote Control Alignment Mirror

III **Sample Chamber**
i Sample Focus
j Reference Focus

IV **Detector Chamber**
k Near, Mid, or Far-IR Detectors

Figure 4.3 Schematic of the IBM-IR/98 BRUKER interferometer

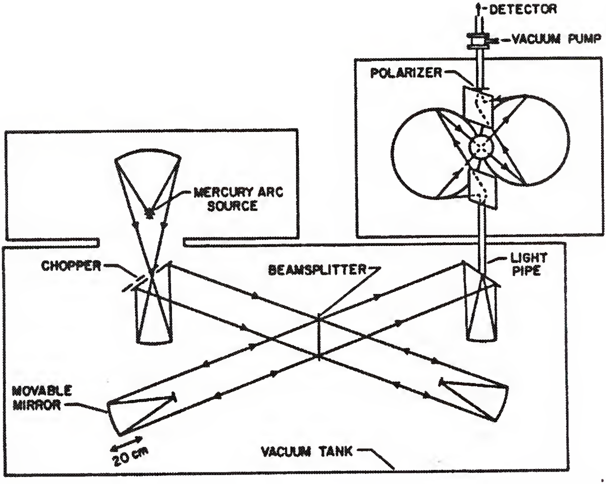

Figure 4.4 Michelson interferometer used in this work

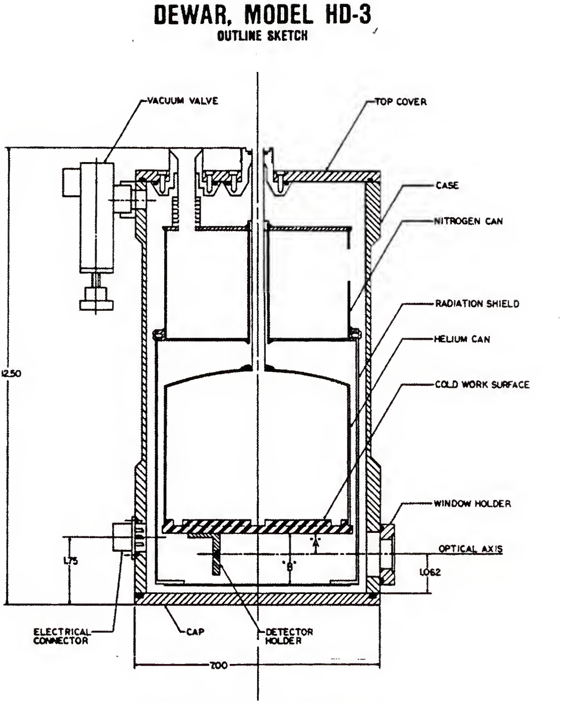

Figure 4.5 Schematic of the Bolometer detector (all dimensions are in inches)

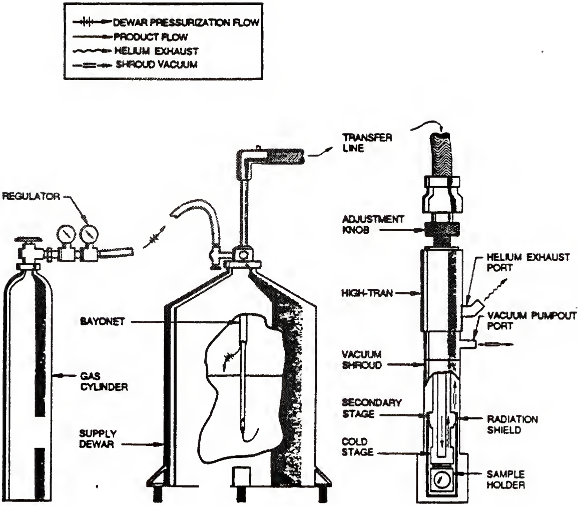

Figure 4.6 Liquid–He flow during the low temperature measurements
(not to the scale)

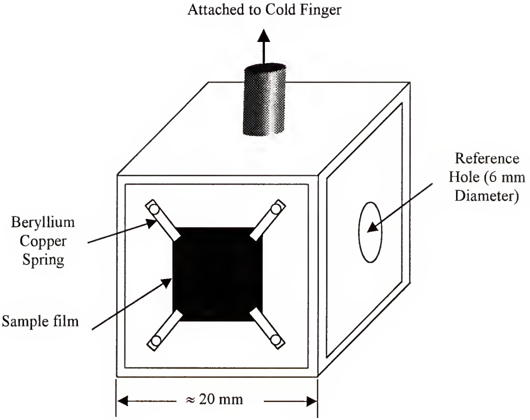

Figure 4.7 Schematic of the sample holder

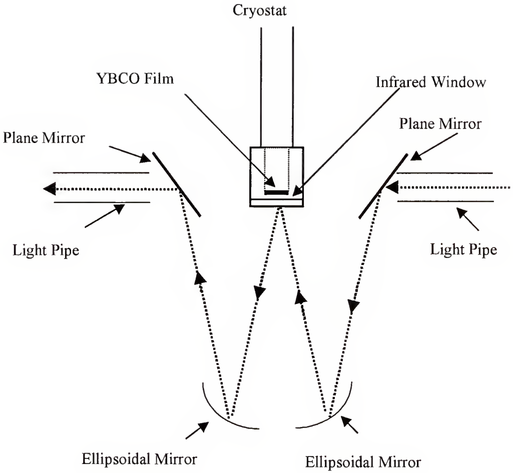

Figure 4.8 Schematic of the reflectance measurement arrangement

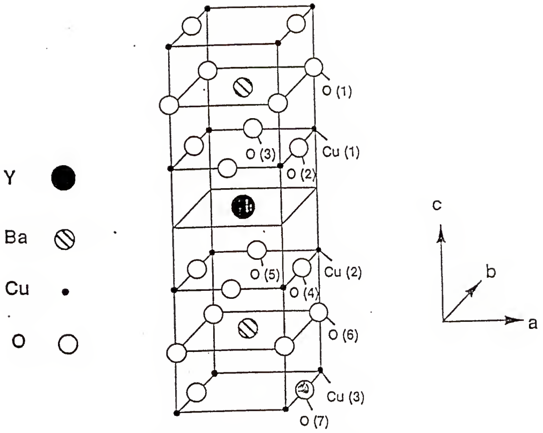

Figure 4.9 Crystalline structure of YBCO

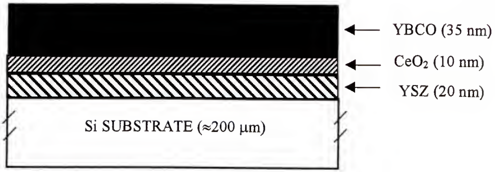

Figure 4.10 Structure of the film-substrate composite
(the lateral dimensions are $\approx 12\times12$ mm^2)

CHAPTER 5
TRANSMITTANCE AND REFLECTANCE

This chapter presents the measured transmittance and reflectance spectra of the YBCO films. The transmittance was measured over the frequency range 10 to 100 cm^{-1} and the reflectance was measured over the range 20 to 640 cm^{-1} at temperatures 10, 50, 100, and 200, and 300 K. The thickness of the YBCO film is ~ 35 nm so the film was transparent enough that the interference features associated with the Si substrate were seen in the measured transmittance and reflectance spectra. Consequently, the measured results were analyzed assuming the film-substrate composite is a thin film on a thin substrate. The dielectric function of YBCO material was modeled by using the Drude–Lorentz model in the normal state, and the two-fluid model in the superconducting state. Details of computing the transmittance and reflectance of film-substrate composite are given in the chapter 3. Analyzed results include the fitted spectra, calculated dielectric function of YBCO and discussions on the antireflection and resonance effects.

Low temperature measurements were also carried on a Si plate that was similar to those served as the substrate for the deposition of the YBCO films. Measurements on Si were done in order to study the effect of temperature on its refractive index. On several occasions, the measurements on Si served as a tool to cross check the alignment of the spectrometers. Before presenting results on the YBCO films, some measurements and analysis on the Si are presented.

Measurements of a Si Substrate

The transmittance and reflectance of the Si substrates were measured at different temperatures to evaluate the refractive index and measurement uncertainty. The refractive index of single-crystal Si has been well documented. The use of the high-resistivity single-crystal Si has essentially eliminated absorption in the substrate. The measured transmittance at 10, 100 and 300 K is presented in Fig. 5.1. The measured transmittance shows interference patterns with T_{max} about 1, T_{min} about 0.3, and a free spectral range $\Delta\omega$ (the frequency interval between two interference maxima) about 7 cm^{-1}. Even a small variation in the substrate thickness (d_{Si}) or its refractive index (n_{Si}) can affect $\Delta\omega$, since $\Delta\omega = (2n_{Si}d_{Si})^{-1}$. The Si thickness is determined from the free spectral range by assuming that $n_{Si} = 3.42$ at frequencies from 10 to 100 cm^{-1} (Loewenstein et al., 1973).

The actual angles of incidence in the transmittance measurement have a spread up to 18° as a result of the beam divergence in the light pipe. The effect of inclined incidence on $\Delta\omega$ (and hence d_{Si}) is less than 0.5 percent since the angle of refraction inside the silicon is small. The transmittance extrema shift toward higher frequencies as the temperature decreases, indicating a decrease of the refractive index since the thickness change can be neglected (Loewenstein et al., 1973). Figure 5.2 presents the measured reflectance along with the measured transmittance at 300 K. For the same Si wafer, the transmittance maxima become the reflectance minima at this temperature, similar trend is also expected at all other temperatures. The measured transmittance was compared with the calculated transmittance to determine the refractive index at different temperatures. The results are $n_{Si} \approx 3.405$ at 200 K, 3.395 at 100 K, and 3.39 at 50 K and 10 K.

Although the interference patterns in the measured transmittance and reflectance of the Si substrate match theoretical predictions as shown in Fig. 5.3 for 300 K, the radiometric accuracy is not as high. The maximum transmittance often varies between 0.95 and 1.05 or more near the spectral cut-offs. The reflectance minimum is always greater than zero, which may be caused by insufficient spectral resolution. The root-mean-square difference between the measured and the calculated values shows a standard uncertainty of ≈ 0.05 in both the transmittance and reflectance. Hence, the uncertainty is estimated to be 10 percent for all measurements. This uncertainty is large compared with the measurements without sharp interference fringes, which could be caused by many parameters, such as detector nonlinearity, misalignment, phase error, and multiple reflections between the sample, windows, and the beam splitter (Griffiths and de Haseth, 1986).

Measurements of YBCO Films

Transmittance

Transmittance was measured using the slow-scan Michelson interferometer. Figure 5.4 shows the measured transmittance of two specimens, identified as Sample A and Sample B, at various temperatures. The transmittance spectra oscillate periodically due to interference effects inside the substrate with $\Delta\omega$ slightly higher than 7 cm^{-1}. In the normal state, the fringe-averaged transmittance, defined as $\overline{T}(\omega) = \frac{1}{\Delta\omega}\int_{\omega-\Delta\omega/2}^{\omega+\Delta\omega/2} T(\omega')d\omega'$, is nearly uniform for all the measured frequencies at any given temperature but decreases gradually as the temperature is lowered. This decrease is expected because the electrical conductivity of the YBCO film increases as temperature decreases. The interference pattern is quite periodic over the studied frequency range at any given temperature, but varies significantly as the temperature is changed from 300 K to 100 K. Not only do the peak locations vary with temperature but also the fringe contrast (the relative amplitude of oscillation) changes significantly. There is a phase shift of π rad between the 300 K and 100 K data; that is, the transmittance maxima at one temperature correspond to the transmittance minima at the other.

The spectrum at 200 K for Sample A has no discernible interference fringes, which can be attributed to an antireflection effect of the YBCO film. Similar feature can be observed for Sample B at a temperature between 200 and 300 K. In the superconducting state, the fringe-averaged transmittance is lower at smaller frequencies and increases toward higher frequencies. The peak transmittance is higher at lower temperatures. This is caused by the optical resonance effect in the film-substrate composite and by decreased absorptance losses in the YBCO film. The antireflection effect on the interference pattern and the effect of optical resonance on the peak transmittance in the superconducting state are discussed in later sections.

Backside Reflectance

The measured backside reflectance spectra of Sample A have been presented in two ways: In Fig. 5.5 spectra are presented along with the interference pattern over the frequency range 10 cm^{-1} to 100 cm^{-1}. In Fig. 5.6 the fringe-averaged spectra over the frequency range 10 cm^{-1} to 640 cm^{-1}, are presented. Both the Fig. 5.5 and Fig. 5.6 reveal that below 100 cm^{-1} the normal state reflectance differs significantly compared to that of the superconducting state. The reflectance increases sharply as the temperature is reduced to below the critical temperature and increases slightly as the temperature is further reduced. The fringe contrast is much higher in the superconducting state than in the normal state.

In a way similar to the transmittance, the fringe contrast is much smaller at 200 K than at 300 K and 100 K. At frequencies where the transmittance is maximum, the reflectance for radiation incident on the substrate decreases to minimum values. The large change in the reflectance of YBCO films at particular frequencies, from the superconducting to the normal state, experimentally demonstrate that HTSC films can be used to construct far-infrared intensity modulators (Zhang et al., 1998).

The fringe-averaged backside reflectance shown in Fig. 5.6 is independent of the frequency in the normal state, but increases toward smaller frequencies in the superconducting state. At frequencies above 150 cm^{-1}, the normal state and superconducting state reflectance are essentially the same. This is corresponds to the superconducting gap above which the radiative properties do not change with the frequency.

Film Side Reflectance

Film side reflectance in the normal state was measured along with the transmittance and backside reflectance measurements. Figure 5.7 shows the measured film side reflectance of Sample A at 100, 200, and 300 K. Here the fringe contrast and the fringe-averaged reflectance are larger compared to the backside reflectance. The spectra at 200 K show no antireflection feature. For the film side incidence, light travels from the low dense medium (air) to high dense medium (silicon) hence the anti reflectance (admittance matching approach) can not observed for this case.

The superconducting state measurements on Sample A were conducted eight months later, gave lower reflectance values than the theoretical calculations. The YBCO film properties are very sensitive to the oxygen content in the film. Oxidation of the films over a period of time might have resulted in loss in the superconducting nature of the film and subsequently films have become less reflective and more transparent. Film side reflectance in the superconducting state, was measured for several samples from another batch. The measured spectra give expected trend and good indication of how the film side reflectance deviates from the backside reflectance. In the superconducting state, the fringe contrast for the film side reflectance become very small compared to that of the backside reflectance. In the analysis section, film side reflectance in the superconducting state is presented for Sample A.

Analysis of Transmittance and Reflectance of YBCO Films

Fitting Procedure

The film-substrate composite consists of a YBCO layer of 35 nm thickness, 20 nm thick YSZ layer, and a 10 nm thick CeO_2 layer deposited on a ~200 μm thick Si substrate. Radiative properties of such multilayer structure can be computed using the matrix method discussed in the chapter 3. Far-infrared wavelengths are comparable with or greater than the substrate thickness, interference fringes are usually observed. During our studies of the Si substrate large interference fringes were observed in measured reflectance and transmittance. The thickness of the film is of the order only 35nm, so the film is essentially transparent and the measured transmittance and the reflectance of the film-substrate composite showed interference fringes. The absorption of dielectric materials, such as YSZ and CeO_2 is very weak in the far-infrared region, especially for thickness less than 20 nm. The dielectric constant of YSZ is 25 and that of CeO_2 is 17 in the far-infrared and microwave regions (Grischkowsky and Keiding, 1990; Phillips, 1996). The presence of the YSZ and CeO_2 layers has essentially no effect on the calculated transmittance and reflectance of the film-substrate composite. Therefore, the YSZ and CeO_2 layers can be omitted while computing the transmittance and reflectance. Based on all details mentioned above, it is justifiable to assume that total film structure consists of a thin film on a thin substrate and simplified formulae for computing reflectance and transmittance can be derived. Using suitable dielectric function models, the complex refractive index of the YBCO film is determined by fitting the measured transmittance data. Because the transmittance measurement has a better spectral resolution, which is especially important in the region where sharp interference extrema occur. Comparison is also made between the calculated and measured reflectance whenever the data are available.

The normal state data were modeled using the Drude-Lorentz model. Due to the relatively weak effect of the Lorentz term in the far infrared, a single oscillator is used with the parameters fixed to those recommended by Zhang et al. (1994), i.e., $\omega_e = 1800$ cm^{-1}, $\omega_{pe} = 18000$ cm^{-1}, and $\gamma_e = 5400$ cm^{-1}. The effect of the mid-infrared band on the radiative properties of the film is very weak at frequencies between 10 and 100 cm^{-1}, because $\varepsilon_{Lorentz}$ is essentially a real constant, $\approx (\omega_{pe}/\omega_e)^2$ in the far infrared. Calculations using different Lorentz parameters, such as $\omega_e = 1800$ cm^{-1}, $\omega_{pe} = 24150$

cm^{-1}, $\gamma_e = 7500\ cm^{-1}$ (Flik et al., 1992), do not modify significantly the transmittance and reflectance of the film-substrate composite.

In the normal state, in order to compute the Drude term, σ_{dc} and $1/\tau$ are taken as adjustable parameters. Their values are determined by fitting the calculated transmittance to the measured transmittance. Calculations show that the radiative properties depend strongly on σ_{dc} but weakly on $1/\tau$, suggesting a larger uncertainty in $1/\tau$. The best fit is obtained when the root-mean-square difference is the smallest. In some cases, the differences in the fringe-averaged transmittance and the peak transmittance are also used to determine the best fit when the root-mean-square difference is not so sensitive to the parameters. The plasma frequency was calculated using the room temperature fitted parameters. The plasma frequency is proportional to the total electron density and is typically constant over temperature (Kamarás et al., 1990; Tanner and Timusk, 1992). Hence, at other temperatures in the normal state, the scattering rate is the only adjustable parameter. In the superconducting state, both the superconducting-electron fraction f_s and the scattering rate $1/\tau$ are considered to be adjustable parameters while computing the dielectric function.

Transmittance

Figure 5.8 compares the fitted and measured transmittance of Sample A. The fitted and measured values agree well with a root-mean-square difference of less than 0.03 in most cases. At temperatures greater than T_c, both the scattering rate and the resistivity drop almost linearly with decreasing temperature. At these temperatures, the scattering rate is dominated by the temperature-dependent electronic scattering, which governs the resistivity dependence on the temperature. Thus, both the resistivity and the scattering rate show a linear dependency on the temperature.

Figure 5.9 compares the fitted and measured transmittance of Sample B. In the normal state the fitted spectra at 100 and 300 K agree well with the measured spectra. Because of the linear temperature dependency, at 200 K, the fitted resistivity is expected to be approximately in between those of at 100K and 300 K. However, the obtained resistivity does not show this trend. There was a large variation from the expected temperature dependency and this required further analysis of the measured spectra. The measured spectra at 200 K were increased by 20 percent and the fitting to this data gave a resistivity, which showed an expected trend. It is strongly believed that some error may have been introduced while measuring the reference spectra at 200 K and this has caused reduction in the measured reflectance.

The fitting parameters for both sample films are shown in Table 5.1. The difference in the fitted values may be caused by the slight variation in the film deposition conditions. At temperatures below T_c, the temperature-dependent scattering ceases to exist, and the remaining scattering is mainly due to impurities and lattice defects, which should be temperature independent (Flik et al., 1992). This scattering rate should be constant at low temperatures. However, the best agreement between the measured and calculated transmittance at 10 K for both the samples was achieved with a scattering rate, which is higher than that for 50 K. This unexpected higher scattering rate at lower temperatures needs further investigation, although it could simply be caused by the experimental uncertainty. Bonn et al. (1992) showed that the scattering rate of YBCO decreases drastically as the temperature is reduced below T_c, due to the rapid reduction of

Table 5.1 Fitting parameters, where the uncertainties are estimated to be 5 percent in $1/\sigma_{dc}$, 20 percent in $1/\tau$, and 10 percent in f_s.

		Sample A ($T_c = 81.5$) $d_{si} = 203.6\ \mu m$ $\omega_p = 6700\ cm^{-1}$			Sample B ($T_c = 80.2$) $d_{si} = 204.3\ \mu m$ $\omega_p = 7500\ cm^{-1}$		
Temp. (K)	n_{Si}	$1/\sigma_{dc}$ ($\mu\Omega$-cm)	f_s	$1/\tau$ (cm^{-1})	$1/\sigma_{dc}$ ($\mu\Omega$-cm)	f_s	$1/\tau$ (cm^{-1})
300	3.420	800	-	600	630	-	600
200	3.405	538	-	400	460	-	440
100	3.395	306	-	230	290	-	275
50	3.390	-	0.25	150	-	0.30	180
10	3.390	-	0.35	190	-	0.40	220

the density of thermally activated quasiparticles. Their results, however, were for a single-crystal $YBa_2Cu_3O_7$ of extremely high quality with $f_s \approx 1$ at very low temperatures.

Even at very low temperatures, there is a large fraction ($1- f_s$) of normal-state electrons in the thin YBCO films. For conventional superconductors, f_s should be zero at temperatures much lower than T_c. The definition of f_s for HTSC materials is rather ambiguous. Some researchers obtained higher values of f_s by assuming a portion of the YBCO film is not superconductive, also known as "dead layer" (Renk, 1992; Hadni et al., 1995). In the present study, the superconducting fraction is calculated without assuming any dead layer, and this may account for the small values of f_s obtained in this study. Another reason may be the higher dc resistivity ($1/\sigma_{dc}$) of YBCO films in the normal state. The dc resistivity is strongly affected by the choice of the substrate and buffer layers, by their thicknesses, as well as by the thickness of the YBCO film (Mechin et al., 1996). The damage caused by the stripping process as mentioned in the chapter 4 may have reduced f_s as well. Although the critical temperature of Sample A is slightly higher than that of sample B, the fraction of superconducting electrons of Sample A is less than that of sample B. This may be explained by the fact that Sample A has a higher electrical resistivity.

Refractive Index of the YBCO

Figure 5.10 and 5.11 show the real and imaginary parts of the refractive index of Sample A and B calculated from the dielectric function, which was obtained by fitting the transmittance data. In the normal state, $n_f \approx \kappa_f$, as expected for a metallic film, and both n_f and k_f increase with decreasing temperature. As the film becomes superconducting, n_f drops suddenly but κ_f exhibits an abrupt increase, especially at low frequencies. As the temperature is further reduced from 50 K to 10 K, n_f continues to decrease whereas κ_f continues to increase. Below T_c, $k_f >> n_f$; because the film is largely inductive in its response. Refractive indices at 10 K of both samples, are compared in Fig. 5.12. In the superconducting state, for Sample B, the imaginary part κ_f is greater and the real part n_f is smaller than those of Sample A. This is due to a slightly larger fraction of the superconducting electrons in Sample B compared to the Sample A (see Table 5.1). This suggests that Sample B is a higher quality film.

Reflectance

The reflectance spectra were calculated using above obtained dielectric function. Figure 5.13 compares the measured with the calculated reflectance for radiation incident on the substrate at 10 and 50 K. The measured and calculated reflectance is in reasonable agreement. For the measurements at 10 and 50 K, at the reflectance minima, the calculated values are much lower than those measured, which may be caused by insufficient resolution in the measured reflectance or by the beam divergence. Further improvements in spectral resolution are required in order to resolve the discrepancy between the measured and calculated reflectance. The reflectance from the substrate side and the film side at 300 K are compared to the calculated spectra in Fig. 5.14. The goodness of fit agreement at 300 K indicates the reliability of the fitted parameters. The calculated film side reflectance for various temperatures is shown in Fig. 5.15. For the incidence on the film side, the locations of the reflectance maxima and minima depend little on temperature in the normal state, but shifts significantly from the normal state to the superconducting state. The fringe contrast decreases as the temperature is reduced, and is an indication of the reduction in the radiation penetration depth in YBCO film with temperature.

Discussion

The Antireflection Effect

For Sample A, measurements reveal that the minima in the transmittance at 300 K approximately correspond to the maxima at 100 K, 50 K, and 10 K. The measured transmittance at 200 K has no discernible interference fringes. This interesting change in the interference pattern is analyzed below by considering the radiation incident from the substrate and reflected by the film. The reflection coefficient at the substrate-film interface as shown in Fig. 5.16 is the ratio of the reflected to the incident electric waves (Heavens, 1965):

$$r = \frac{-r_{23} + r_{21}e^{i2\delta_f}}{1 - r_{23}r_{21}e^{i2\delta_f}} \tag{5.1}$$

where, for normal incidence, $r_{21} = (N_2 - N_1)/(N_2 + N_1)$ and $r_{23} = (N_2 - N_3)/(N_2 + N_3)$, and $\delta_f = \omega d_f N_2 / c_0$ is the complex phase change in the film. Note that $N_1 = 1$, $N_2 = N_f$, and $N_3 = n_{Si}$ correspond to the refractive indices of the air, film, and the substrate, respectively, and c_0 is speed of light in vacuum. If $|2i\delta_f| << 1$, which is satisfied for the thin YBCO film in the normal state, then $\exp(2i\delta_f) \approx 1 + 2i\delta_f$. The requirement of $|2i\delta_f| << 1$ is equivalent to (1) $d_f << \lambda / 4\pi k_f$ (the film thickness is much smaller than the radiation penetration depth), where λ is the wavelength in vacuum, and (2) $d_f << \lambda / 4\pi n_f$. After some manipulation, Eq. (5.1) becomes

$$r \approx \frac{N_3 - N_1 + i\delta_f N_2(1 + N_3/N_2)(1 - N_1/N_2)}{N_3 + N_1 - i\delta_f N_2(1 - N_3/N_2)(1 - N_1/N_2)} \tag{5.2}$$

Assume $|N_1 / N_2| << 1$ and $|N_3 / N_2| << 1$, which are also valid since the refractive index and extinction coefficient of metallic films (such as YBCO in the normal state) are generally much greater than the refractive index of dielectric materials (such as the Si substrate used here). Then,

$$r \approx \frac{N_3 - N_1 + i\delta_f N_2}{N_3 + N_1 - i\delta_f N_2} \tag{5.3}$$

Equation (5.3) is the same as that derived by McKnight et al. (1987), but here it is obtained directly from Maxwell's equations without assuming that the film is infinitely thin. It is convenient to define a dimensionless admittance, $y = -i\delta_f n_f$, which in general is a complex quantity. As discussed above, the dielectric function of YBCO in the normal state is dominated by the Drude term, which becomes purely imaginary at frequencies much smaller than the scattering rate ($\omega\tau << 1$); hence, $\varepsilon(\omega) \approx i\sigma_{dc}/\omega\varepsilon_0$. From the definitions of y and δ_f, $y \approx \sigma_{dc} d_f / c_0 \varepsilon_0$ is a real positive constant in the very far infrared. When $y = n_{Si} - 1$, the reflection coefficient given by Eq. (5.3) becomes zero for incidence on the substrate. For $N_3 = n_{Si} \approx 3.4$, the required dc resistivity ($1/\sigma_{dc}$) is ≈ 550 μΩ-cm for $d_f = 35$ nm. The dc resistivity obtained by fitting the transmittance at 200 K of 538 μΩ-cm is very close to this value. However, because the scattering rate is only 400 cm^{-1} at 200 K (see Table 5.1), there are residual interference fringes. Because of all the assumptions made earlier, interference fringes persist in the calculated transmittance even with $1/\sigma_{dc} \approx 550$ μΩ-cm. McKnight et al. (1987) analyzed and experimentally demonstrated the effect of antireflection coating (also called impedance-matched coating) on the transmittance of a Si wafer coated with a Ni-Cr film. In that work, the scattering rate was much greater than 100 cm^{-1}, and the fringe contrast in the measured transmittance was much smaller.

The change from transmittance maxima at 300 K to transmittance minima at 100 K at fixed frequency can be explained by the sign change of the reflection coefficient given by Eq. (5.3) as the dc resistivity passes ≈ 550 μΩ-cm. The change in the sign of this coefficient, combined with the interference effect inside the Si substrate, will result in a phase shift of π rad in the interference pattern and thus causing the transmittance to change from maxima to minima and vise versa. The calculated transmittance and reflectance agree extremely well in terms of the interference patterns at all temperatures except for Sample A at 200 K. The actual phase at 200 K is very complicated because the assumptions used in deriving Eq. (5.3) are not perfectly met. The discrepancy in the phase between the calculated and the measured transmittance at 200 K may also suggests that the scattering rate is complex and may depend on the frequency. Modified Drude models with a complex and frequency-dependent scattering rate have been used for the study of HTSC materials (Varma et al., 1989; Virosztek and Ruvalds 1990; Renk, 1992; Quinlan et al., 1996). Further studies are needed to investigate the applicability of these models to thin YBCO films on Si substrates.

The fringe patterns of Sample B differs from those of Sample A, because their characteristics are different. From Fig. 5.4 and Table 5.1, we can estimate that the interference contrast for Sample B would be the smallest at a temperature somewhere between 300 K and 200 K, where its dc electric resistivity is near 550 $\mu\Omega$-cm. The condition for impedance matching with the Si substrate is that $(\sigma_{dc} d_f)^{-1} \approx 157\,\Omega$. Hence, it is possible to construct antireflection coatings with a YBCO film on Si substrate at room temperature by increasing the film thickness. The practical applications of the antireflection effect using HTSC films need further exploration.

The Effect of Optical Resonance

The measured spectra for both specimens at 10 K and 50 K have sharper transmittance maxima and reflectance minima than the spectra obtained above the critical temperature. In addition, the peak transmittance at 10 K is even higher than that at 50 K. The transmittance is expected to decrease as the temperature is lowered since the YBCO material becomes more and more conductive. The unexpected higher transmittance at lower temperatures in certain spectral bands is the result of optical resonance in the film-substrate composite. A simple optical resonator is a dielectric layer coated with highly reflecting films on both sides. By varying the reflection coefficient of one or both coatings, the transmittance of the resonator can be altered significantly. This resonance effect will result in very high transmittance values at particular frequencies. In the present study, the specimen is analogous to an optical resonator made of a thin YBCO film coated on only one side of the Si substrate. As the temperature is reduced to below the critical temperature, the reflection coefficient of the YBCO film increases sharply. The large reflection coefficient, coupled with the interference effects in the substrate, can significantly increase the measured transmittance at certain frequencies. The observed resonance effects demonstrate that YBCO films deposited on Si substrates have the potential for construction of Fabry-Perot resonators (Renk et al., 1990; Genzel et al., 1992; Malone et al., 1993). Further discussion on resonance structures using Sample A and B, is presented in chapter 7.

Sensitivity of the Fitting Parameters

In the present work, only the measured transmittance was used for obtaining the dielectric function of the YBCO material. The reflectance of the film was calculated using the above-obtained dielectric function. In the far-infrared limit, the dc resistivity and scattering rate are sufficient to model the dielectric function in the normal state. In Table 5.2, the dc resistivity and scattering rate at 300 K and 100 K reported by several groups are compared with the present work. These values vary in a range of about 200% due to different preparation methods and different substrates. Calculations show that the radiative properties depend strongly on $1/\sigma_{dc}$ but weakly on $1/\tau$, suggesting a larger uncertainty in $1/\tau$. Uncertainty in the fitted $1/\tau$ and $1/\sigma_{dc}$ is evaluated by observing

Table 5.2 The dc resistivity and scattering rate obtained by different groups.

Authors & Year.	Substrate	d_f (nm)	ρ_{dc} ($\mu\Omega$-cm)		$1/\tau$ (cm^{-1})	
			300 K	100K	300 K	100 K
Kumar et al. 1999c	Si	35	800	306	600	230
Gao et al. 1991	MgO	48	555	165	550	175
Flik et al. 1992	$LaAlO_3$	10	880	-	300	-
		25	420	-	400	-
Cunsolo et al. 1993	MgO	50	390	150	480	180
Phelan et al. 1992	MgO	35	860	-	270	-

change in the transmittance introduced by variation of these parameters. Figure 5.17 shows the fitted transmittance for the Sample B at 100 K along with the transmittance computed with ± 20 percent change in $1/\tau$ and ± 5 percent change in $1/\sigma_{dc}$. The large change in the scattering rate has little effect on the transmittance indicating a larger percentage of uncertainty in the fitted values. However, the transmittance is very sensitive to change in the dc resistivity. As indicated by Fig. 5.17 even a ± 5 percentage change can introduce a large variation in the fitted transmittance.

In the superconducting state, best fitting was obtained with f_s between 0.25 and 0.4. The existence of normal electrons at very low temperatures has been noticed by many authors (Tanner and Timusk 1992). The fraction of superconducting electrons at 10 K was about 0.5 obtained by Gao et al.(1991) for a 48 nm thick YBCO film and by Flik et al. (1992) for a set of films (10 to 200 nm thick). The value of f_s was between 0.70 and

0.85 for single crystals and thick films at temperatures much less than T_c (Zhang et al., 1994). This indicates that the quality of the YBCO film deposited on the Si substrate used for the present study can be further improved.

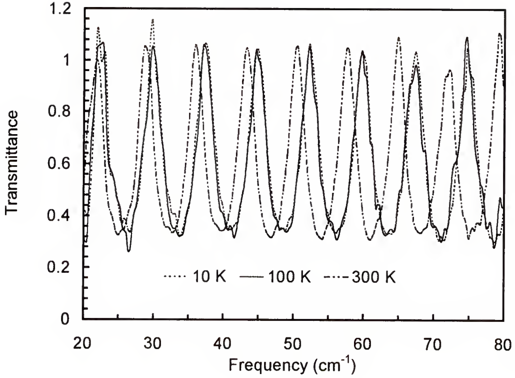

Figure 5.1 Measured silicon transmittance at different temperatures

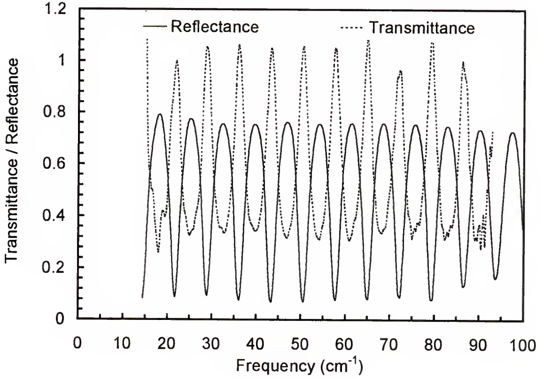

Figure 5.2 Measured silicon reflectance and transmittance at 300 K

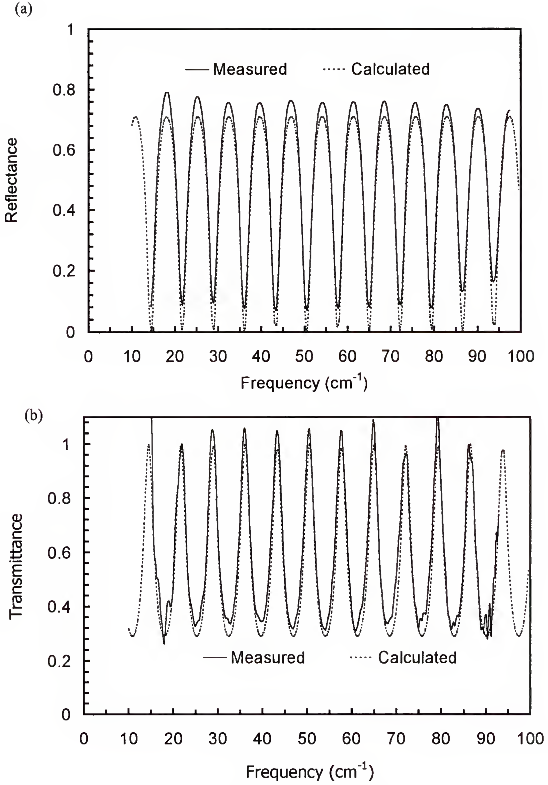

Figure 5.3 Comparison of measured and fitted (a) Reflectance (b) Transmittance of Si

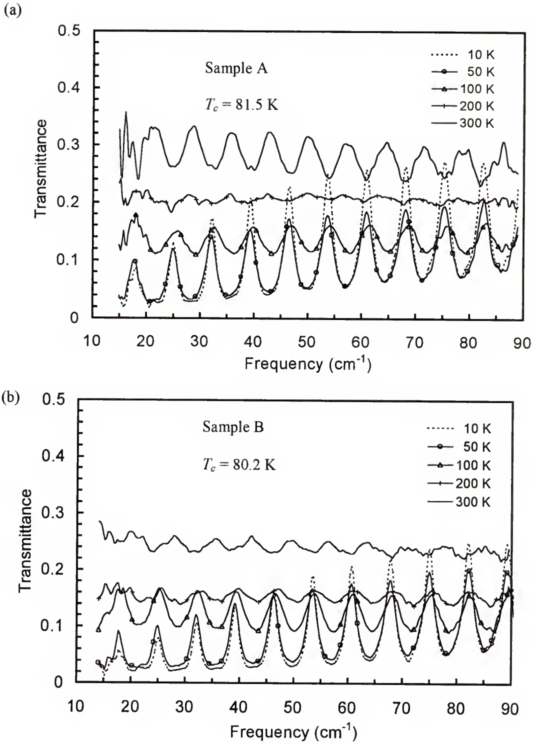

Figure 5.4 Measured transmittance of YBCO films on Si substrates

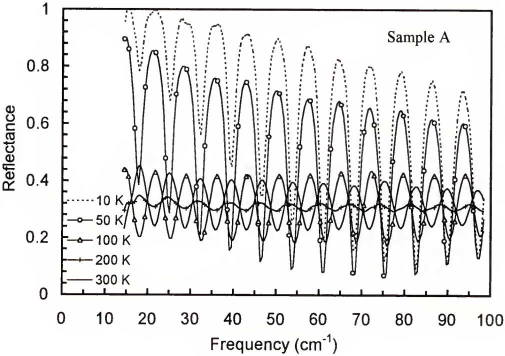

Figure 5.5 Measured reflectance for radiation incident on the substrate (backside)

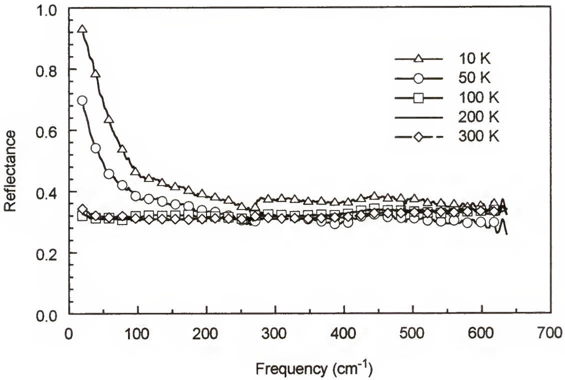

Figure 5.6 Fringe-averaged backside reflectance

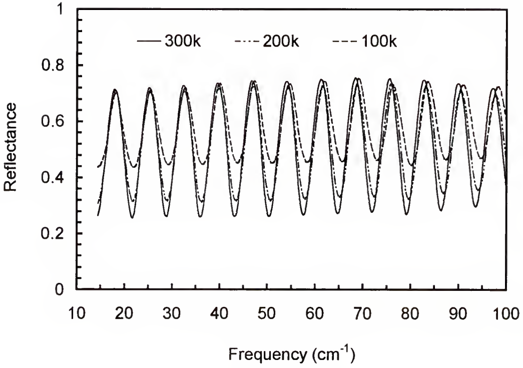

Figure 5.7 Measured film side reflectance in the normal state

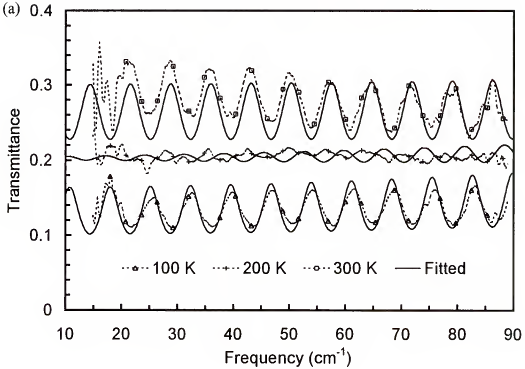

Figure 5.8 Comparison between the measured and fitted transmittance for Sample A: (a) normal state; (b) 50 K; (c) 10 K.

(b)

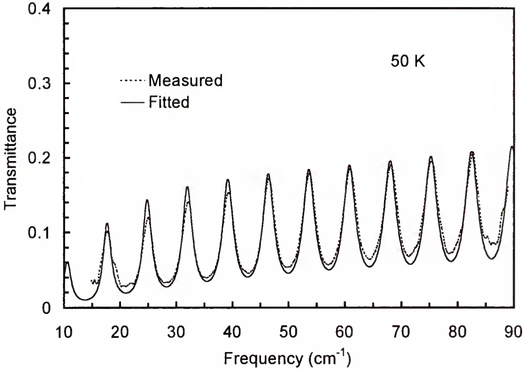

(c)

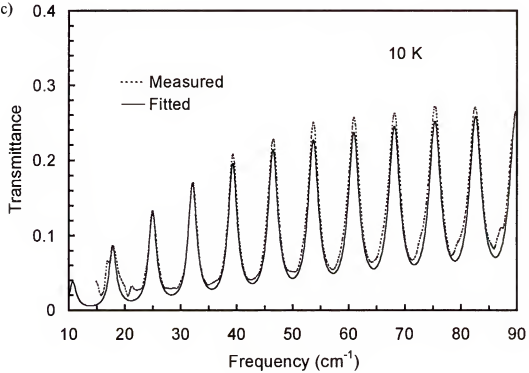

Figure 5.8 -- continued

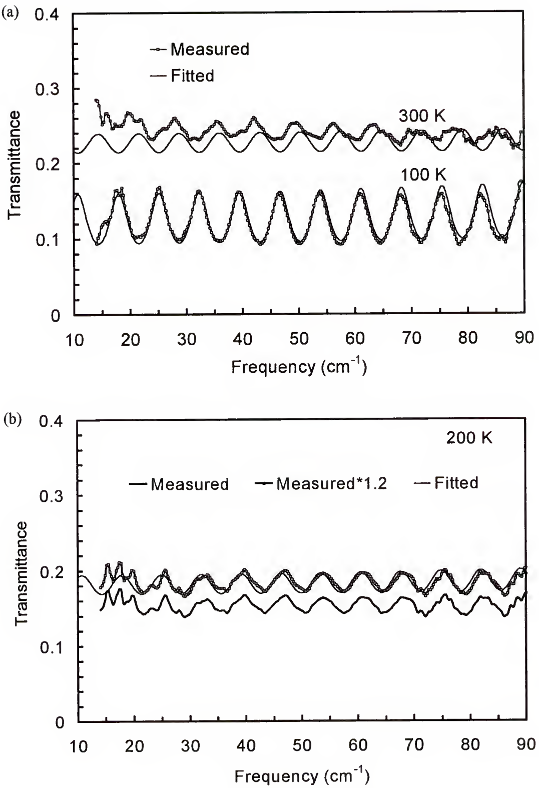

Figure 5.9 Comparison between the measured and fitted transmittance for Sample B: (a) 100 and 300 K; (b) 200 K; (c) 50 K; (d) 10 K

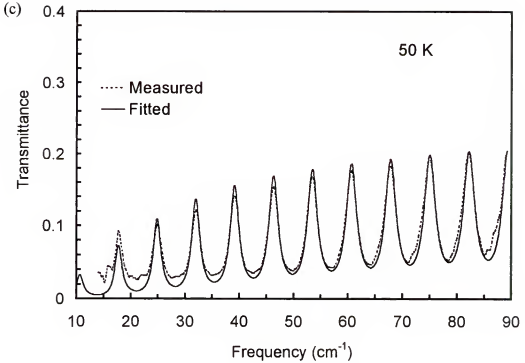

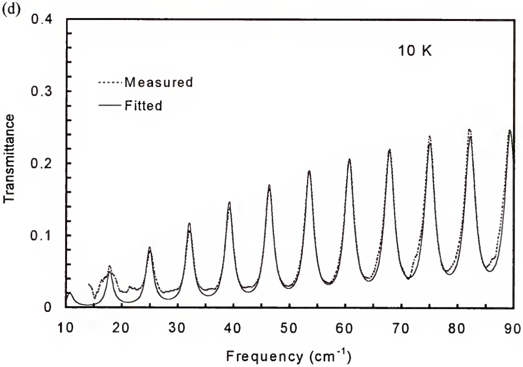

Figure 5.9 -- continued

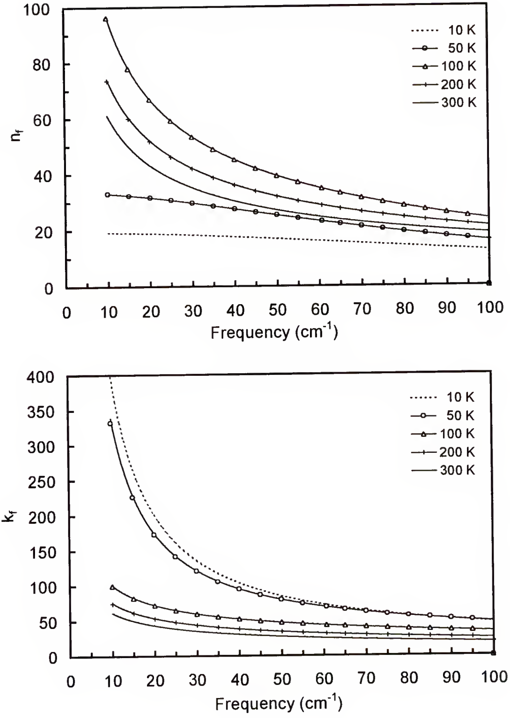

Figure 5.10 Complex refractive index of the YBCO film (Sample A)

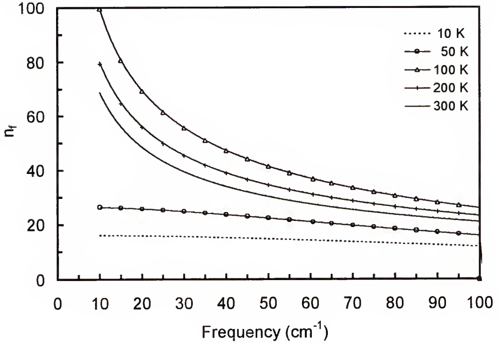

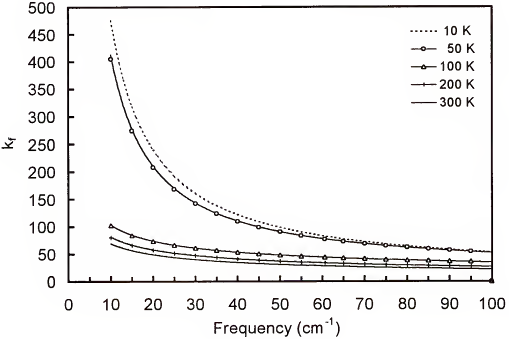

Figure 5.11 Complex refractive index of the YBCO film (Sample B)

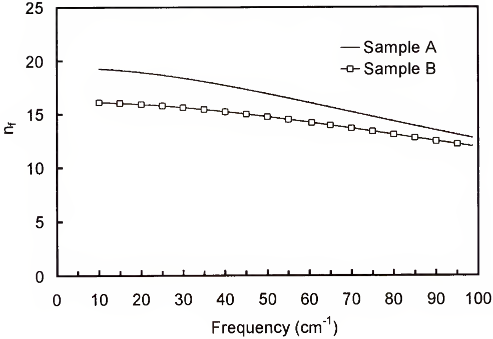

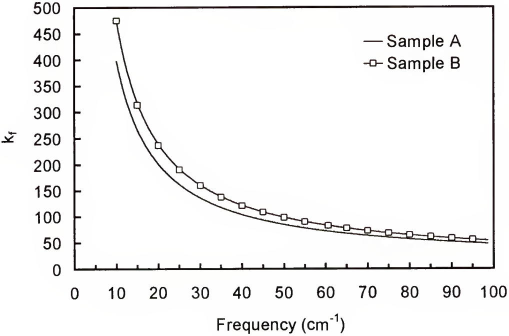

Figure 5.12 Comparison between the refractive index of Sample A and B at 10 K

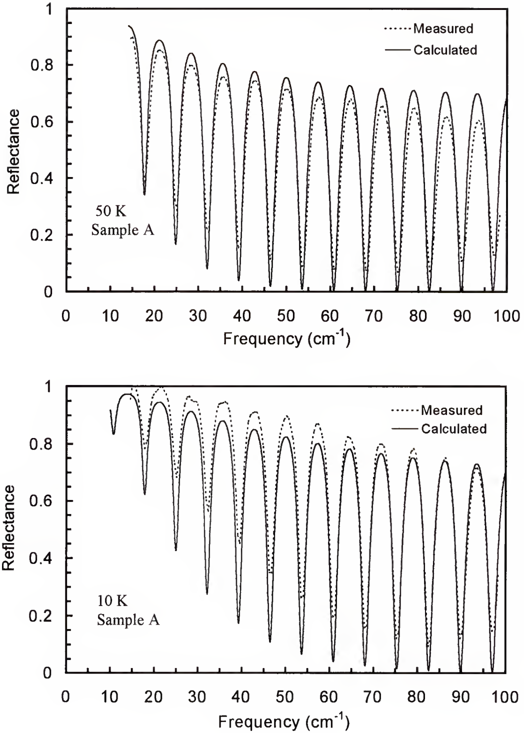

Figure 5.13 Measured and calculated backside reflectance for Sample A at 50 K and 10 K

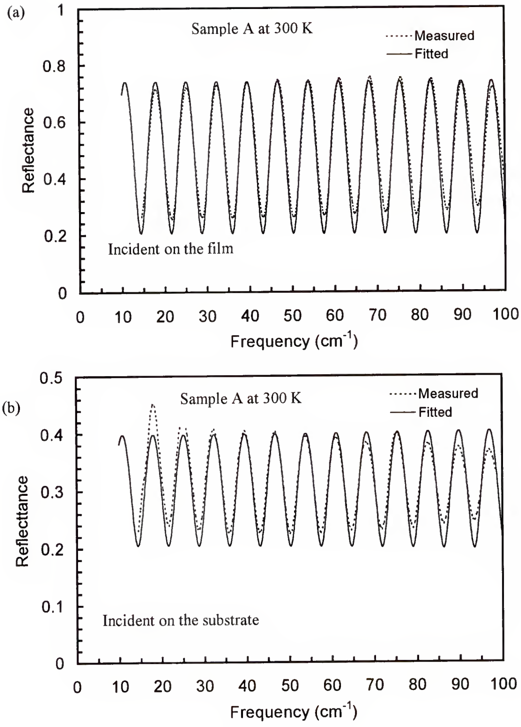

Figure 5.14 Comparison between the measured and calculated reflectance at 300 K for radiation incident (a) on the film; (b) on the substrate

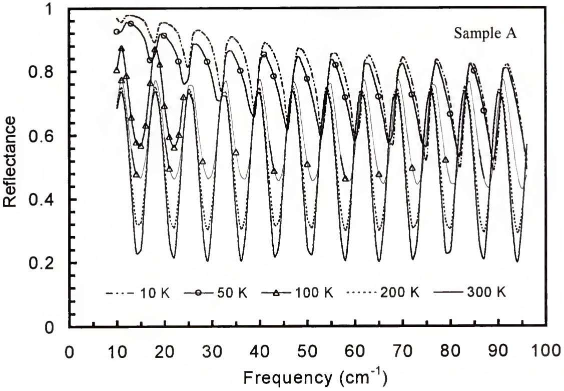

Figure 5.15 Calculated film side reflectance

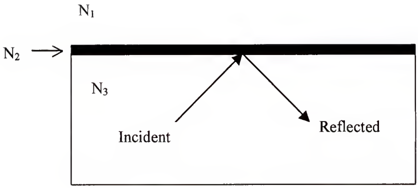

Figure 5.16 Substrate incident reflection coefficient

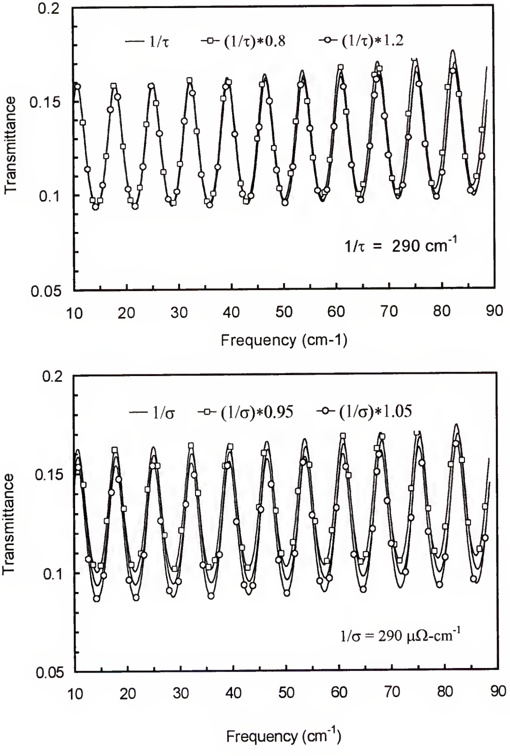

Figure 5.17 Effect of uncertainty in the fitted parameters on the fitted transmittance (a) Scattering rate; (b) dc resistivity

CHAPTER 6
ABSORPTANCE OF YBCO FILMS

This chapter presents the normal state absorptance of YBCO films in the frequency region 10 to 100 cm^{-1}. The absorptance spectra were presented both for the radiation incident on the film side and the backside. The measured transmittance and reflectance spectra were used in computing the absorptance spectra. Results show that the absorptance for radiation incident on the film side differs significantly from that for radiation incident on the substrate side. The dielectric function obtained from the transmittance measurements was used to study the effect of the film thickness on the total absorptance of the film-substrate composite.

HTSC thin films have been used to construct highly sensitive infrared–radiation detectors. These detectors operate above the liquid–nitrogen temperature using an HTSC thin film as the sensing element. Knowledge of the amount of the radiation absorbed within the film is crucial for the detector design. A larger absorptance yields a higher responsivity and detectivity as well as a smaller noise equivalent power (Carr et al., 1990, Zhang and Frenkel, 1994). The absorptance of the HTSC film depends not only on the wavelength of the incident radiation and temperature of the film–substrate composite but also on the thickness of the film and properties of the substrate. Higher absorptance occurs when the radiation is incident on the substrate side. Silicon is an ideal substrate for the fabrication of HTSC bolometers because of its higher thermal conductivity and infrared transparency. Phelan et al. 1992, investigated the thickness–dependent absorptance of YBCO films deposited on MgO substrates, in the frequency region 100 cm^{-1} to 200 cm^{-1}. Studies show that the absorptance by very thick films, is small compared to that of thin films and there exists an optimum thickness for which absorptance is maximum in the film-substrate composite (Kumar et al., 1998).

Results

Figure 6.1 shows the measured absorptance of Sample A at various temperatures for radiation incidence on both the film side and the substrate side. The interference pattern is independent of the frequency except at 300 K. The measurement errors associated with the 300 K transmittance data, are cause for the slight decrease in the absorptance below 40 cm^{-1}. The spectrum at 200 K for the backside illumination shows no distinct interference fringes but for the film side illumination at the same temperature, the fringe pattern can be observed clearly. The phase shift of π rad between the 300 K and 100 K spectra is similar to the one observed in transmittance spectra. The fringe-average absorptance presented in Table 6.1. indicates that the absorptance for the backside illuminations is higher than for the film side illumination and similar trend is also expected in the superconducting state. The measured reflectance for the film side is always greater than for the backside illumination (Fig. 5.5 and Fig. 5.7) and the transmittance is the same in both cases (Fig. 5.4a), hence the absorptance is greater for the backside illumination. The higher absorptance in the detector element- an important criterion required for the design of radiation detectors, can be achieved through the backside illumination.

Table 6.1 Fringe averaged absorptance in the normal state for radiation incident on the film side (A_f) and the backside (A_s)

Temperature (K)	A_f	A_s
100	0.30	0.55
200	0.29	0.48
300	0.21	0.40

Normal state absorptance is calculated using the calculated transmittance and reflectance spectra. The measured spectra are compared to the calculated spectra in Fig. 6.2. The predicted and measured absorptance values match closely, considering the experimental uncertainty, except for the interference pattern at 200 K. The actual phase at the 200 K is very complicated to model and complexity may be due to experimental noise or may be due to the losses in the Si substrate.

Effect of the Film Thickness

The effect of the film thickness on the absorptance was studied by varying the value of d_f, the film thickness. Figure 6.3 shows the predicted absorptance at 100 K between 40 cm^{-1} and 60 cm^{-1} for five different values of d_f. The film thickness has a significant effect on the absorptance, especially for the backside illumination. The increase in the thickness makes the film more opaque. The competing effects of a decrease in the transmittance and an increasing reflectance result in an optimized d_f where the absorptance is maximum.

For a bare Si substrate, the transmittance maximum (T_{max}= 1) and the reflectance minimum (R_{min} = 0) are located at $\omega = m\Delta\omega$, where m is an integer and the free spectral range $\Delta\omega = (2 n_S d_S)^{-1} = 7.234 \mathrm{cm}^{-1}$ with $n_S = 3.395$ and $d_S = 203.6$ μm. The location of T_{min} and R_{max} are located at $\omega = (m + 1/2)\Delta\omega$. The maximum in A_f is located near $m\Delta\omega$ and remains at that location for all the calculated thicknesses. Similarly the minimum in α_f is remain located near $(m + 1/2)\Delta\omega$. The fringe-averaged absorptance and fringe contrast increases with the film thickness up to 20 nm, and then decreases as d_f is further increased.

The maximum of A_s is located at $m\Delta\omega$ for $d_f < 20$ nm, and switches to $(m + 1/2)\Delta\omega$ for $d_f > 20$ nm. Note that $d_f = 20$ nm causes an antireflection effect at the film-substrate interface. The maximum and the fringe-averaged values of A_s continues to increase as the film thickness is increased beyond $d_f = 20$ nm. The fringe-averaged absorptance reaches a maximum value 0.6 and the peak absorptance reaches a maximum value 0.9, when $d_f = 70$ nm. Further calculations show that the maximum absorptance can be achieved for d_f between 90 and 120 nm. Figure 6.2 shows that $A_s = A_f$ at $\omega = m\Delta\omega_s$.. Considering that the transmittance is same both for the film side and the backside illumination, it can be concluded that the film side and backside reflectances should be the same at $\omega = m\Delta\omega$. This can also be shown that $R_f = R_S$ if $\phi = m\pi$, i.e., $\exp(i 2\phi_S) = 1$. The existence of frequencys where $R_f = R_S$ can be used in practice to check the measurement uncertainty.

The change in the absorptance can be understood better by plotting the transmittance and reflectance at 6.5 $m\Delta\omega_s$ and $7m\Delta\omega_s$, as shown in Fig. 6.4. Note That T decreases but R_f increases as d_f increases. When $r_b = 0$, which corresponds to $d_f \approx 20$ nm, Rs is approximately 0.3 and independent of frequency. Because the wave reflected by backside of the film interferes with the wave reflected by the surface of the substrate, R_S at 47.02 cm^{-1} continues to decrease as d_f is further increased above 20 nm. At frequencys equal to $(m+1/2)\Delta\omega$, there exists a minimum R_S when $d_f \approx 90$ nm.

Absorptance in the Superconducting State

The absorptance in the superconducting state is calculated using the fitting parameters obtained from the transmittance measurements (see Table 5.1). Calculated superconducting state absorptance for Sample A for radiation incidence on the substrate side and on the film side is shown in Fig. 6.5 and 6.6, respectively. The superconducting state absorptance shows a uniform fringe-pattern except at very low frequencies similar to the transmittance and reflectance. The absorptance maxima of the backside incidence and film side incidence are located at slightly different frequencies.

Both the A_s and A_f decreases as the temperature is lowered. Decrease in the temperature causes the superconducting fluid fraction, f_s, to increase (see Table 5.1). In the superconducting state, the absorptance is mainly due the residual normal state electrons whose number is proportional to $1-f_S$. Thus, the decrease in $1-f_S$ results in decrease in the absorptance.

Between 40 cm^{-1} and 100 cm^{-1} the fringe-averaged A_f and A_s are smaller in the superconducting state than in the normal state. The fringe-contrast decreases for A_f but increases for A_s. At particular frequencies the value of A_s is as high as 0.8 but at low frequencies it is much lower than that of the normal state. Therefore, when the superconducting films are employed as the detector element at very low frequencies, some coating may be required to enhance its absorptance.

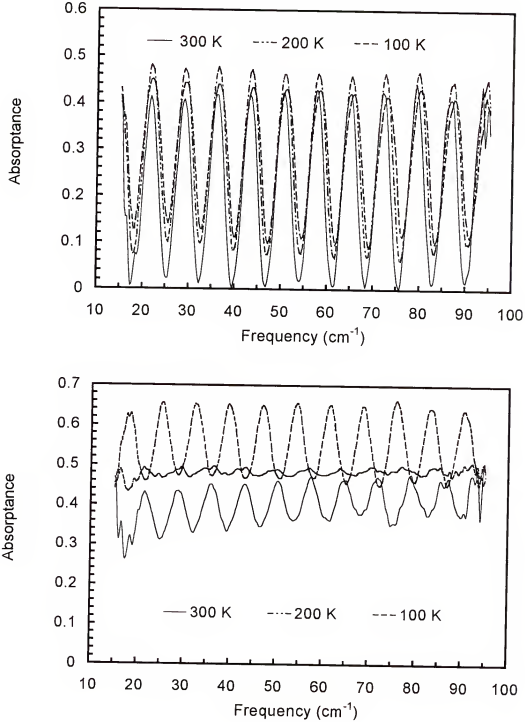

Figure 6.1 Measured absorptance of YBCO film for radiation incident on (a) the film side (b) the substrate side

(a)

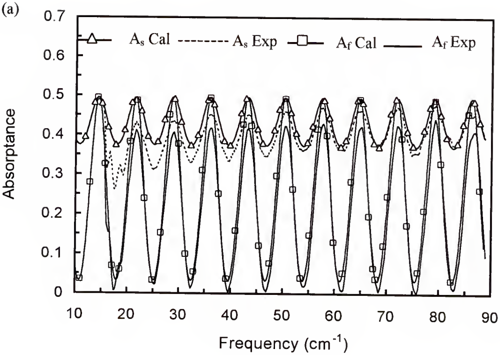

(b)

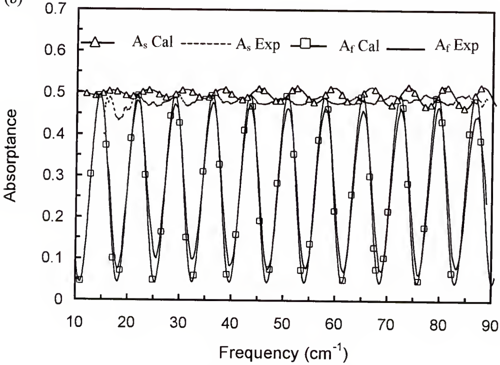

Figure 6.2 Comparison between the measured and calculated absorptance at (a) 300 K (b) 200 K (c) 100 K

(c)

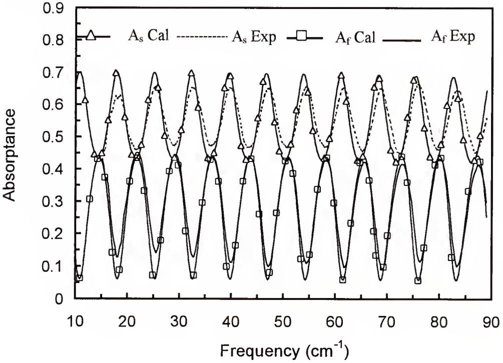

Figure 6.2 --continued

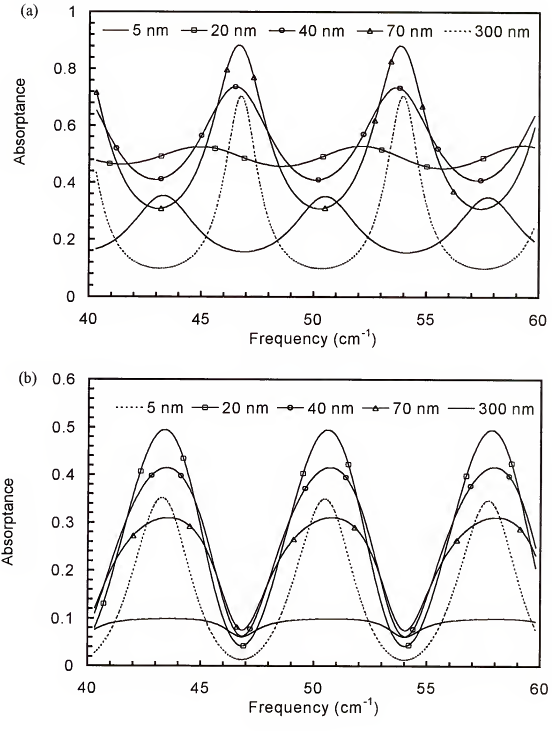

Figure 6.3 Calculated absorptance at 100 K for radiation incident on
(a) the substrate side (b) the film side

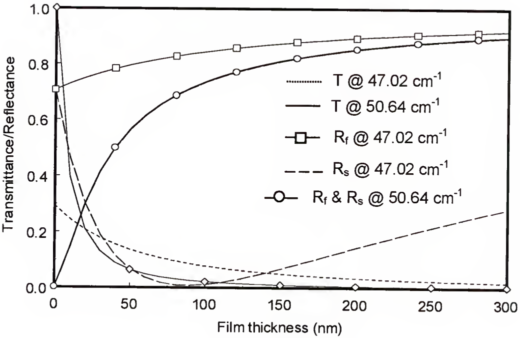

Figure 6.4 Effect of the film thickness on the transmittance and reflectance

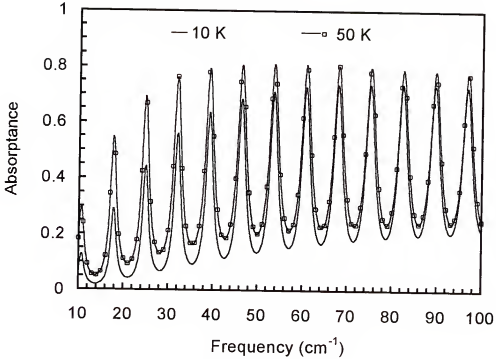

Figure 6.5 Calculated substrate incident absorptance in the superconducting state

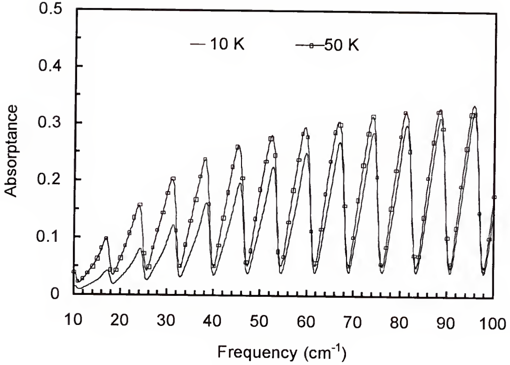

Figure 6.6 Calculated film side incident absorptance in the superconducting state

CHAPTER 7
FABRY-PEROT RESONATORS

Results and analysis of the optical resonators built with HTSC thin films are presented in this chapter. The operational details of the Fabry-Perot (F-P) resonators were introduced in Chapter 3. Experiments were carried on two sets of resonator structures. The F-P resonator was built using the Sample A and B, whose transmittance and reflectance were discussed in Chapter 5, as reflectors. The transmittance of the resonator structure was measured at temperatures of 10, 50, 100, 200 and 300 K in the frequency region from 10 to 90 cm^{-1}.

The chapter begins with theoretical analysis of the resonator transmittance. A comprehensive survey of the previous studies conducted on the F-P resonators built from HTSC thin films are presented in the next section. Experiments are described along with the observations on the measured transmittance characteristics. Later, the comparisons are presented between the measured and calculated transmittance. Finally, in the discussion section the resonance transmittance optimization and effect of the YBCO film thickness are presented.

Theoretical Background

A simple plane F-P resonator consists of two parallel mirrors separated by a gap, with their reflecting surfaces facing each other. In the present experiments, two Si substrates coated with YBCO films were used to form an F-P resonator as shown in Fig.

7.1. The transmittance through this multilayer structure was derived using the two-effective-interface method described Chapter 3. The transmittance of the resonator is given by Eq. (3.42). After some algebraic manipulations

$$\mathcal{T} = \frac{\dfrac{T_1 T_2}{(1-\sqrt{R_1 R_2})^2}}{1+\dfrac{4\sqrt{R_1 R_2}}{(1-\sqrt{R_1 R_2})^2}\sin^2\left(\dfrac{\beta+\phi_1+\phi_2}{2}\right)} \tag{7.1}$$

where subscripts 1 and 2 indicates the first and the second film/substrate composite, T and R are the transmittance and the film-side reflectance of the composite, $\delta = 4\pi\omega d$ is the phase shift of the radiation at frequency ω for one round trip inside the cavity of length d with a refractive index equal to 1, and ϕ is the phase shift upon refection at the film surface. Equation (7.1) can be expressed in a more compact form using the definitions of the finesse,

$$F = \frac{\pi (R_1 R_2)^{1/4}}{1-\sqrt{R_1 R_2}} \tag{7.2}$$

and the resonant transmittance,

$$\mathcal{T}_{res} = \frac{T_1 T_2}{(1-\sqrt{R_1 R_2})^2} \tag{7.3}$$

Hence, the transmittance of the resonator is

$$\mathcal{T} = \frac{\mathcal{T}_{res}}{1+\dfrac{4F^2}{\pi^2}\sin^2(\dfrac{\psi}{2})} \tag{7.4}$$

where $\psi = \delta + \phi_1 + \phi_2$. The transmittance reaches its maxima ($\mathcal{T}_{res}$) for $\psi = 2m\pi$ and its minima for $\psi = (2m+1)\pi$ where m is the order of the interference fringe. If the change in

$\mathcal{T}_{\text{res}}$ is small, the locations of the half maxima can be calculated by setting the denominator in Eq. (4) to be 2, i.e., $F^2 \sin^2(\psi/2) = \pi^2/4$. For larger values of F, ψ values are $\psi = 2m\pi \pm \pi/F$. If changes in ϕ_1 and ϕ_2 are neglected, the bandwidth measured by the full width at half maximum (FWHM) is $(2dF)^{-1}$. This is consistent with the definition of the finesse F, which is the ratio of the fringe separation or the free spectral range, $\Delta\omega = (2d)^{-1}$, to the bandwidth. For a given cavity length, F is inversely proportional to the bandwidth of the transmittance peak. The effects of interference inside the substrate are included in the T and R terms, which can cause additional oscillations (sidebands) in the transmittance spectra and/or interfere with the resonant transmittance peaks. Hence, the actual bandwidth and finesse may differ significantly from the simplified calculations. It is noteworthy that the transmittance of the resonator can also be calculated using the transfer-matrix method described in Chapter 3 (Malone et al., 1993; Kumar and Zhang, 1999). Because Eqs. (7.2) - (7.4) clearly distinguish the influence of the cavity resonance from the properties of each individual reflector, they are employed in the present analysis.

Review of F-P Resonators Built with HTSC Thin Films

High-temperature superconducting (HTSC) thin films on transparent substrates have been considered as a potential substitute for the metallic mesh reflectors in far-infrared resonators (Renk et al., 1990). Metallic meshes show absorption at infrared frequencies due to the ohmic losses from the current induced in the wires (Belland and Lecullier, 1980). This absorption within the metallic mesh limits the finesse of the resonators. In the superconducting state, superconducting thin films have no ohmic losses (i.e., no absorption) for frequencies up to their superconducting energy gap, which lies in the far-infrared region for HTSC material. Hence, the F-P resonators built with HTSC thin films should offer a higher finesse than those with metallic meshes, although some residual absorption still exists at low temperatures due to non-condensing electrons. Another advantage is the suppression of high-frequency radiation, as HTSC materials are more opaque than the metallic-mesh at high frequencies (Renk et al., 1990).

Renk et al. (1990) reported the use of HTSC thin films for the construction of F-P resonators in the frequency range up to 300 cm^{-1}. They used 100 nm thick YBCO films on 1 mm thick MgO substrates as reflectors and a cavity length of 44 μm. The obtained peak transmittance was $\approx$0.016 with a finesse $F \approx 30$ for the first-order resonance. The lower transmittance was due to the relatively thick YBCO film. Wiese et al. (1992) measured the transmittance of a resonator made from two reflectors: a 50 nm thick YBCO film on a 0.35 mm thick MgO substrate and a 70 nm thick YBCO film on a 0.25 mm thick MgO substrate. The reported peak transmittance was $\approx$0.16 and $F \approx 55$ for the first-order resonance located near 80 cm^{-1}. In order to obtain a high peak transmittance, the HTSC films should be thin enough so that they do not block all the radiation and the substrates should effectively transmit in the frequency region of interest. Pechen et al. (1992) measured the transmittance of a resonator built from 30 nm thick YBCO films deposited on 0.5 mm thick Si substrates. The measured peak transmittance at 10 K was about 0.6 with $F \approx 20$ at the first-order resonance frequency of $\approx$60 cm^{-1}. Although this peak transmittance is much higher than that obtained in the previous studies, the resonance in the substrates has caused strong sidebands that overlap the main resonance peaks (Pechen et al., 1992). The smaller thickness of the substrate used in the work by Kumar et al., (1999a) allows the distinction of the main resonance from the sidebands caused by interference effects in the substrates.

Experiments

In the present study, Sample A and B are used as reflectors to built the F-P resonator. The transmittance and reflectance characteristics of these samples were presented in Chapter 5. The spacer that separates the two films was either a polyimide sheet of 132 μm thickness or a copper plate of 550 μm thickness, with a hole at the center. The cross-sectional view of the resonator arrangement is shown in Fig. 7.1. The distance between the two films, i.e., the cavity length d, is determined by the spacer. The sample holder shown in Fig. 4.7 was used for the transmittance measurements. Slightly curved beryllium copper strips, fastened with screw on the corners of one plate, act like springs to hold the films along with the spacer to the copper plate. The transmittance spectra were measured using the slow-scan Michelson interferometer.

The measured transmittance spectra for the polyimide spacer are shown in Fig. 7.2. The transmittance peaks resulting from the resonance within the cavity are located at $\omega_m = m/2d$, where m = 1, 2, ... Therefore, the transmittance peaks of the first- and second-order resonance for this spacer are approximately located at 39 cm^{-1} and 76 cm^{-1}, respectively. The actual resonance frequencies are determined by ψ, which is influenced by ϕ_1 and ϕ_2. The resonant transmittance peaks are shifted toward higher frequencies as the temperature is lowered. This can be explained by the decrease in the refractive index of the Si substrate as the temperature is lowered. The resonance (or interference) within the Si substrates is coupled to the main resonance inside the cavity, resulting in complex fringes. The sidebands include additional transmittance peaks near the main resonance and ripples in the spectra.

Above 100 K the peak transmittance associated with sidebands is comparable to that of the main resonance. In the normal state $\mathcal{T}_{\text{res}}$ decreases with temperature, by a factor of two from 300 to 100 K. If both the YBCO films were identical, then $\mathcal{T}_{\text{res}}$ given by Eq. 7.3 can be expressed as (Renk and Genzel, 1962)

$$\mathcal{T}_{\text{res}} = \frac{1}{(1 + \mathrm{A}/\mathrm{T})^2} \tag{7.5}$$

where $\mathrm{A} = 1 - \mathrm{T} - \mathrm{R}$ is the absorptance of the film/substrate composite. The smaller the value of A/T, the higher the resonant transmittance $\mathcal{T}_{\text{res}}$. The YBCO material exhibits a metallic behavior in the normal state. Its electrical conductivity will increase as the temperature decreases, yielding a reduction in the transmittance and an increase in the reflectance. The absorptance for radiation incident on the film side does not change significantly with temperature in the normal state (Kumar et al., 1999b). Therefore, as the temperature is lowered, the resonant transmittance decreases whereas the finesse increases, which means a decrease in the bandwidth. The transmittance associated with the sidebands show a relatively higher percentage of reduction than the main resonant transmittance, because the increase in the reflectance of the YBCO films has suppressed the interference effects within the Si substrates.

In the superconducting state, however, the sidebands are significantly suppressed in comparison with the main resonance and this difference becomes even larger at the second-order resonance. Another feature associated with the superconducting state is that at some locations, the peak transmittance increases as the temperature is lowered. This is particularly true at the second-order resonance (76 cm^{-1}), where $\mathcal{T}_{\text{res}}$ is increased from 0.24 at 50 K to 0.28 at 10 K. Similar characteristic was observed in the transmittance spectra of a single film/substrate composite due to the resonance in the Si substrate (see Fig. 5.4). The radiative properties of YBCO in the superconducting state differ greatly from those in the normal state. In the superconducting state, HTSC materials tend to show perfect reflection and little absorption for radiation at frequencies below its energy gap. Decreasing the temperature causes an increase in the fraction of superconducting electrons and a decrease in the far-infrared absorptance (Tanner and Timusk, 1992). Hence, the increase in the peak transmittance from 50 K to 10 K can be attributed to the decrease in the absorptance within the YBCO films. Similar to the normal state, the bandwidth also decreases with the decrease in temperature, because of the increase in the reflectance. The measured finesse at 76 cm^{-1} is approximately 20 at 50 K and 23 at 10 K.

The measured transmittance spectra for the copper spacer are shown in Fig. 7.3. Here, the transmittance peaks resulting from the resonance within the cavity are separated at an interval of ~ 9 cm^{-1} and are located at approximately 9 cm^{-1}, 18 cm^{-1}, 27 cm^{-1}, etc. The transmittance characteristics at different temperatures show the expected pattern as described for the polyimide spacer.

Calculation and Comparison

The transmittance T, film-side reflectance R, and phase shift ϕ of each reflector can be calculated using the optical constants of the film and substrate, assuming it is composed of a thin absorbing film on a thin (coherent) transparent substrate (Kumar et al., 1999b). By comparison with the experiments, best fitting parameters (such as the plasma frequency and scattering rate) were obtained and reported in Chapter 5 for each individual reflector. The fitted parameters obtained for the two films are not the same because of variation in the conditions of deposition and post treatment. There exists a large fraction of residual normal electrons at temperatures below T_c. The buffer layers have negligible effect to either the phase shift or the transmittance and reflectance.

The refractive index of Si depends on the frequency, increasing for about 0.1% from 10 to 100 cm^{-1} (Loewenstein et al., 1973). Such small variation is negligible in the frequency region considered here; therefore, the refractive index of Si is assumed to be dependent only on temperature. The refractive index of Si changes from 3.42 at 300 K to 3.39 at 10 K as obtained by fitting the interference fringes in the transmittance and reflectance spectra of a bare Si substrate. The substrate thicknesses are d_{Si} = 203.6 μm and 204.3 μm for the two reflectors, respectively. Changes in d_{Si} due to thermal expansion are within 0.024% throughout the temperature range, which is negligibly small. The uncertainty in the refractive index and thickness of Si is approximately 0.5%. The surfaces are optically smooth with a root-mean-square roughness of a few nanometers. Because the wavelength is longer than 100 μm, the effect of surface roughness can be neglected.

The transmittance of the resonator is very sensitive to the optical path length introduced by the spacer. The thickness of the polyimide spacer measured with a micrometer was 132 μm. To obtain a good agreement with the measured fringes, in the computation, the cavity length was adjusted to 138 μm at 300 K and 134 μm at 10 K. This discrepancy may be due to the beryllium copper springs not being tight enough.

Excessive tightening was avoided as it might break the samples. As low temperatures, there may be a decrease in the cavity length due to thermal contraction of the polyimide film and the effect of the beryllium copper springs. Notice that the cavity length is the only adjustable parameter in the calculation using Eq. (7.1) or Eq. (7.4).

Another important issue is the parallelism between the two reflecting surfaces. Only manual adjustments were done during experiment to maintain the two reflectors as parallel as possible. Parallelism between the two reflecting surfaces also might have suffered from the uneven tightening of these springs. Equations from thin-film optics are strictly applicable to complete coherent cases but nonparallelism can significantly reduce the fringe contrast and peak transmittance. The effect of partial coherence on the radiative properties of thin films were studied by many authors, see for example Chen and Tien (1992) and Anderson and Bayazitoglu (1996). The finite spectral resolution and beam divergence also reduce the coherence (Zhang, 1994). In the experiments the frequency interval between data points was ≈0.28 cm^{-1} and the spectral resolution was 0.56 cm^{-1}. The spatial incoherence introduced by the nonparallelism and by the beam divergence is frequency dependent (Grossman and McDonald, 1995). Therefore, an empirical relation for the frequency-dependent effective resolution ($\delta\omega$) is introduced as

$$\delta\omega = \sqrt{0.56^2 + (0.02\omega)^2} \tag{7.6}$$

Equation (7.6) gives an effective resolution from about 0.6 to 2.1 cm^{-1} as ω changes from 10 to 100 cm^{-1}. In the computation, the transmittance is integral averaged from $\omega-\delta\omega/2$ to $\omega+\delta\omega/2$ for each point. Figure 7.4 shows the comparison between the measured transmittance and calculated transmittance which includes the effect of partial coherence. The measured and calculated values agree closely except for the spectra at 10 K in the regions from 30 to 37 cm^{-1} and from 65 to 72 cm^{-1}.

The measured and calculated transmittance at 300 K and 10 K for the resonator with the copper spacer is shown in Fig. 7.5. The interference in the Si substrates has a strong effect on the peak transmittance because $\mathcal{T}_{\text{res}}$ changes drastically with frequency, which will be discussed in the following section. The measured peak transmittance is 0.51 at 300 K and 0.16 at 10 K for the second-order resonance. The FWHM bandwidth for this transmittance peak is 1.1 cm^{-1} and 0.9 cm^{-1} at 300 K and 10 K, respectively.

To demonstrate the effect of partial coherence, the transmittance calculated directly from thin-film optics (coherence) with a frequency interval of 0.05 cm^{-1} is compared with that calculated considering partial coherence in Fig. 7.6. The effect of partial coherence is particularly large for sharp transmittance peaks. Notice that the bandwidth of the transmittance peak broadens due to partial coherence. Higher spectral resolution with improved alignment between the two reflecting surfaces should improve the future measurements.

Discussion

Resonant Transmittance Optimization

The radiative properties of individual reflectors, which are related to the interference effects in the substrates, strongly influence the transmittance characteristics of the resonator. The resonant transmittance $\mathcal{T}_{\text{res}}$, determined from Eq. (7.3), depends entirely on the two reflectors not on the cavity length. Figure 7.7 plots the calculated T_1, R_1 and ϕ_1 of the first reflector, together with $\mathcal{T}_{\text{res}}$ at 300 K and 10 K for completely coherent situation. The properties of the second reflector are very similar to these of the first one since the thickness of the substrates is nearly the same (≈204 μm). All spectra oscillate due to interference in the substrate with a period (free spectral range) of $\Delta\omega_{Si} = (2 n_{Si} d_{Si})^{-1}$, where d_{Si} is the thickness and n_{Si} the refractive index of Si. In the normal state, the fringe contrast in the reflectance is much larger than that in the transmittance. Therefore, the maxima of both $\mathcal{T}_{res}$ and R_1 are located at the same frequencies, given by

$$\omega_{m,Si} = \frac{2 m_{Si} + 1}{4 n_{Si} d_{Si}} \tag{7.7}$$

where m_{Si} is the order of resonance in the Si substrate. At frequencies equal to $\omega_{m,Si}$, ϕ_1 is approximately zero. In order to achieve the maximum peak transmittance, the particular resonance in the cavity must be coincident with one of the resonances in the substrates. Since $\phi_1 \approx \phi_2 \approx 0$ at the substrate resonance, Eq. (7.4) suggests that δ must equal $2\pi m$, corresponding to the main resonant frequencies $\omega_m = m/2d$. By equating ω_m and $\omega_{m,Si}$, we have

$$d = \frac{2 n_{Si} m}{2 m_{Si} + 1} d_{Si} \tag{7.8}$$

which is a criterion for obtaining optimal resonant transmittance.

In the superconducting state, Fig. 7b shows that ϕ_1 is always greater than zero and the behavior of T_1 and R_1 are quite different from those in the normal state. The maxima of $\mathcal{T}_{res}$, however, is still located near $\omega_{m,Si}$, where ϕ_1 is close to zero. Therefore, Eq. (7.8) provide a good approximation for maximum performance to be obtained. The actual value of d may be slightly different from that given by Eq. (7.8).

Although Eq. (7.8) was originally obtained by Malone et al. (1993), here it is derived by analyzing the F-P equation and the properties of each individual reflector in detail. Malone et al. (1993) adjusted the substrate thickness in the computation to predict the optimal transmittance. In practice, it is often easier to adjust the cavity length. In our experiments, the value of d was chosen at random and was kept constant. In order to show that HTSC films on transparent substrates are indeed good candidates for far-infrared resonators, the cavity length d is varied to compute the optimal characteristics of the resonator.

The peak transmittance is optimized for the first and second order of the cavity resonance (i.e., m = 1,2) for 10 K. The value of m_{Si} is chosen that the value of d lies in the close vicinity of 134 μm, the value obtained from the experiment. Using $n_{Si} = 3.39$ and $d_{Si} = 204$ μm, which is the average thickness of the two substrates, Eq. (7) gives the values of d that yield the maximum transmittance to be 126 μm ($m_{Si} = 5$) and 133 μm ($m_{Si} = 10$), respectively, for the first- and second-order resonance. The actual optimized cavity lengths are d = 123 μm and 130 μm. Figure 7.8 compares the calculated transmittance for the cavity lengths optimized for the first- and second-order resonance with that obtained from the experiment. All three cases are assumed to be completely coherent. The optimized peak transmittance is near 0.6, which is 400% higher than the peak transmittance for the first-order resonance obtained from the experiment. Another important feature in the optimized situation is that the sidebands have been substantially reduced, which is the advantage of using thin Si substrate as compared with the 0.5 mm thick Si substrates used in the study of Pechen et al. (1992). The value F calculated from Eq. (7.2) also oscillates. Because $\mathcal{T}_{res}$ and ϕ_1 change drastically with frequency, the value of F calculated from Eq. (7.2) is not an indicator of the finesse anymore. The finesse is calculated by dividing $\Delta\omega$ by the FWHM bandwidth.

The above method can be applied to optimize the performance for various ranges of d and at different temperatures. These calculations demonstrate that HTSC materials are promising candidates for constructing far-infrared resonators. The performance of the resonator, however, is a strong function of the cavity length. Therefore, a mechanism that can adjust the cavity length within a few micrometers during the measurement is required and currently under development to achieve the optimize performance.

The Effect of the YBCO Film

The YBCO film thickness affects the transmittance, reflectance, and absorptance of the individual reflectors, which in return affect the transmittance characteristics of the resonator. Increasing the film thickness will decrease the transmittance of the film/substrate composite, yielding a reduction in the peak transmittance of the resonator as can be seen from Eq. (7.3). However, increasing the film thickness will increase the reflectance of the film/substrate composite, which in turn will improve the finesse, see Eq. (7.2).

The effect of the YBCO film thickness is studied by varying its value on one or both reflectors, under conditions that facilitate the maximum possible first-order resonant transmittance as discussed above. The results show that, as the YBCO thickness decreases, the peak resonant transmittance increases and reaches the highest value of unity for zero thickness (i.e., only pure Si substrates). The height of the sidebands also increases as the YBCO film thickness decreases. The bandwidth of the transmittance peaks shows a decreasing trend with the increase in the YBCO film thickness, indicating that the finesse is increasing. Hence, a compromise must be made in the design of F-P resonators between high resonant transmittance and high finesse with suppressed sidebands. The thickness of the YBCO film should generally be equal to or less than 50 nm. The quality of the YBCO film also affects the resonator's performance. High-quality films with little residual absorption in the superconducting state will improve the peak transmittance and finesse.

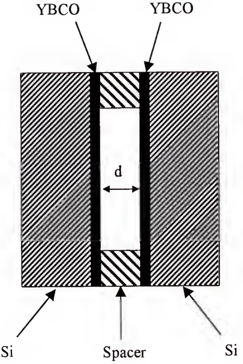

Figure 7.1 The cross-sectional view of the resonator structure (not to scale)

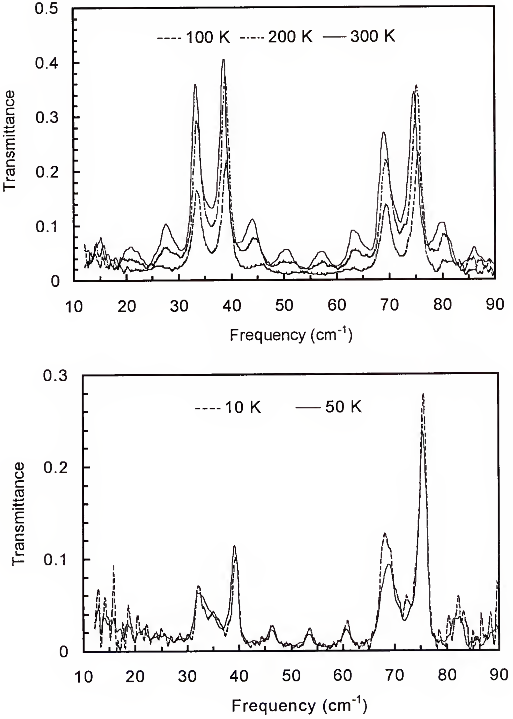

Figure 7.2 Measured transmittance of the resonator (Cavity length d = 132 μm)

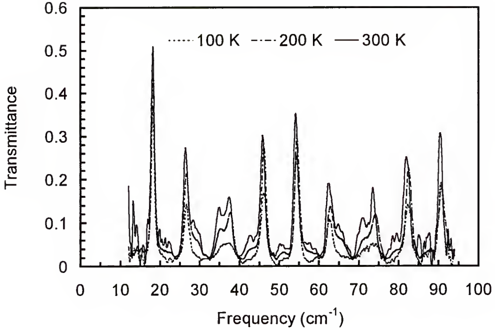

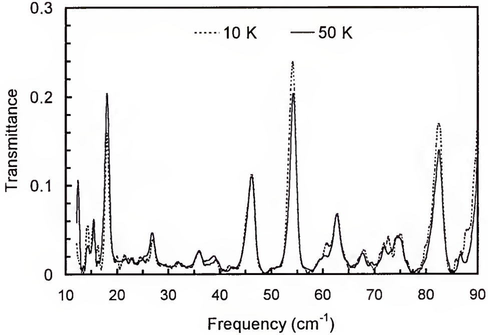

Figure 7.3 Measured transmittance of the resonator (Cavity length d = 550 μm)

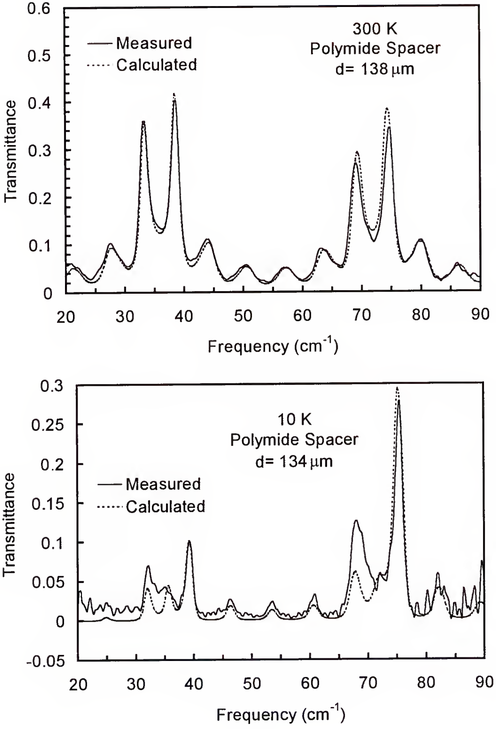

Figure 7.4 Comparison between the measured and calculated transmittance

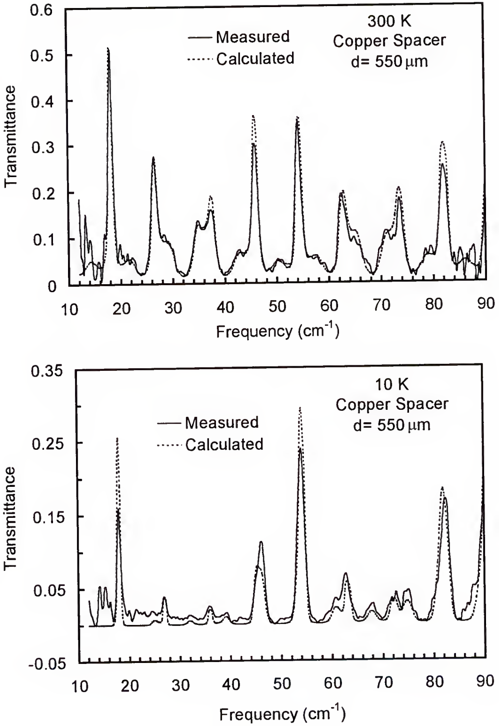

Figure 7.5 Comparison between the measured and calculated transmittance

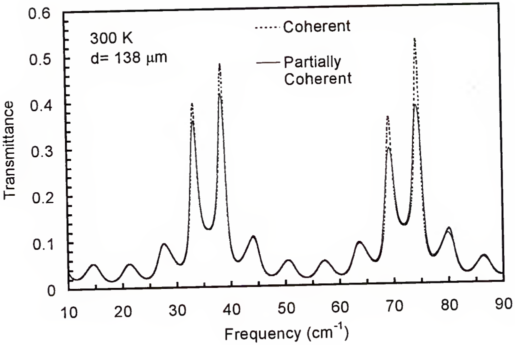

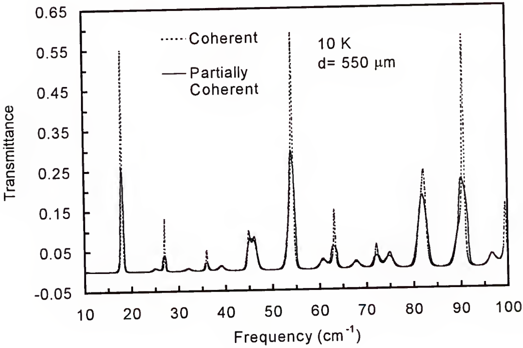

Figure 7.6 The effect of partial coherence on the resonant transmittance.

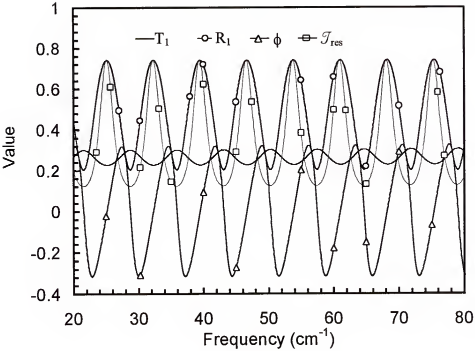

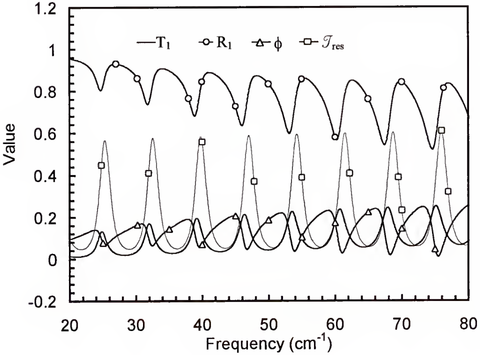

Figure 7.7 Calculated T, R, and ϕ for the first reflector (Sample A) together with $\mathcal{T}_{res}$

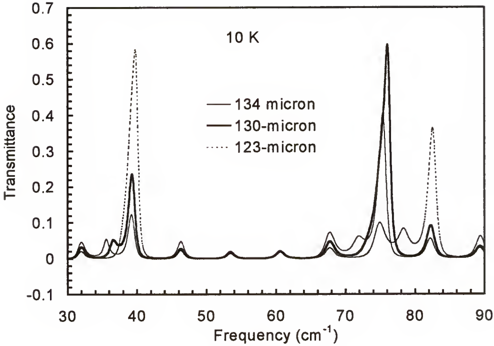

Figure 7.8 The effect of cavity length on the peak transmittance for the first- and second-order resonance.

CHAPTER 8
SUMMARY AND CONCLUSIONS

This dissertation is devoted to an extensive study and analysis of YBCO films deposited on Si substrates. Transmittance and reflectance measurements were carried on several sample films and some important results are presented. Backside reflectance measurements on the film-substrate composite indicate that these films can be used for building far-infrared intensity modulators. Measurements of the Fabry-Perot resonators show that the films deposited on the nonabsorbing silicon have great potential for building high finesse and high transmittance resonators in the far-infrared.

Radiative Properties of the YBCO Films

The transmittance and reflectance of thin YBCO films deposited on transparent Si substrate, were measured in the far-infrared region at temperatures from 10 K to 300 K. The measurements show fringes caused by interference effects within the Si substrate. The change in the dc conductivity of the YBCO film with temperature causes a change in the reflection coefficient at the substrate-film interface, which results in a variation of the interference pattern. Matching of the admittance of the YBCO film with the refractive index of the Si substrate will yield a zero reflection coefficient at the substrate-film interface and thus eliminate the fringes in the measured transmittance. A change in the sign of the reflection coefficient results in a phase change of π rad in the interference pattern.

Sharp increases in the transmittance maxima in the superconducting state indicate that optical resonance has occurred within the film-substrate composite. The reflectance for radiation incident on the substrate increases significantly upon switching from the normal state to the superconducting state. These phenomena demonstrate that the HTSC thin films on transparent substrates can be used to build far-infrared devices such as optical resonators and radiation modulators.

The transmittance and reflectance are calculated using the Drude model in the normal state and the two-fluid model in the superconducting state. The predicted values agree closely with the measured values using only a few adjustable parameters. The complex refractive index of the YBCO films is thus obtained at different temperatures. The imaginary part increases steeply as the superconducting state is reached but the real part shows a sudden decrease. The refractive index of YBCO films obtained from this study is important for the design of promising devices using HTSC thin films.

The measured normal state absorptance and the calculated superconducting state absorptance are presented. The absorptance for backside illumination is greater than that for the radiation incidence on the film side. It is observed that the absorptance is a sensitive function of the film thickness. The effect of the film thickness on the absorptance is studied by calculating the radiative properties as a function of the film thickness. There exists an optimal thickness, for which the absorptance is maximum although such thickness for incident on the film side is different from that incident on the substrate side. At certain frequencies the optimized absorptance for backside incidence can be greater than 0.9. The absorptance data and analysis provided here will facilitate the design of infrared detectors based on YBCO films.

Fabry-Perot Resonators

The transmittance of Fabry-Perot resonators built from YBCO films on Si substrates as the reflecting surface, was measured in the far-infrared region at temperatures between 10 and 300 K. The sidebands observed in previous studies have been suppressed by the use of thin substrates. The resonant transmittance decreases with temperature in the normal state but may increase in the superconducting state as the temperature goes down. The calculated transmittance considering partial coherence is in good agreement with the experimental data.

An optimized analysis was performed to predict the maximum resonant transmittance by examining the interference effects in the cavity and substrates. The transmittance characteristics of the resonator are very sensitive to the thickness of each layer that forms the resonator. The maximum resonant transmittance is obtained when the resonance in the cavity is coincident with that in the substrates. An increase in the YBCO film thickness will improve finesse but reduce peak transmittance.

These measurements demonstrate the potential of using YBCO thin films on thin Si substrates to construct F-P resonators. The simple procedure laid out for calculating the transmittance of the resonators helps in analyzing the effect of a single reflector and the future design of similar resonators.

The film deposition techniques need to be improved in order to make films of similar characteristics. The quality of the YBCO film should be improved to reduce the residual absorption for higher performance. This will be useful for making resonators of required performance. Future work is recommended to use a mechanism that will improve the alignment between the two reflectors and can tune the cavity length during measurement. A high spectral resolution should also be used to discern sharp transmittance peaks.

REFERENCES

Anderson, C.F., and Bayazitoglu, 1996, "Radiative Properties of Films Using Partial Coherence Theory," *J. Thermophys. Heat Transfer*, Vol. 10, pp. 26-32.

Aguiar, R., Sanchez, F., Peiro, D., Ferrater, C., and Varela, M., 1994, " $YBa_2Cu_3O_{7-x}$ Thin Films on Double Buffer Layers on Si(100)," *Physica C*, Vol. 235-240, pp 647-648.

Belland, P., and Lecullier, J.C., 1980, "Scanning Fabry-Perot Interferometer: Performance and Optimum Use in the Far Infrared Range," *Appl. Opt.*, Vol. 19, pp. 1946-1952.

Berberich, B., Chiusuri, M., Cunsolo, S., Dore, P., Kinder, H., and Varsamis, C.P., 1993, "Far-Infrared Spectra of Imperfect YBaCuO Films on Si Substrates," *Infrared Physics*, Vol. 34, pp. 269-279.

Bonn, D.A., Dosanjh, P., Liang, R., and Hardy, W.N., 1992, "Evidence for Rapid Suppression of Quasiparticle Scattering below T_c in $YBa_2Cu_3O_{7-\delta}$," *Phys. Rev. Lett.*, Vol. 68, pp. 2390-2393.

Boyce, J.B., Connell, G.A.N., Fork, D.K., Fenner, D.B., Char, K., Ponce, F.A., Bridges, F., Tramontana, J., Viano, A.M., Laderman, S.S., Taber, R.C., Tahara, S., and Geballe, T.H., 1989, "*In-situ* Growth of Superconducting $YBa_2Cu_3O_y$,Films by Pulsed Laser Deposition," in: *Processing of Films for High T_c Superconducting Electronics* T.Venkatesan, ed., SPIE, Belligham, WA, Vol. 1187, pp. 136-147.

Brodbeck, R., Pepe, F.A., Tognina, C., Bhend, D., Zimmerman, E., and Kneubuhl, F.K., 1998, "Balloon-Borne Far-Infrared Fabry-Perot Spectrometers for Astrophysical Observations," *Infrared Physics and Technology*, Vol. 39, pp. 393-414.

Carr, G.L., Quijada, M., Tanner, D.B., Hirschmugl, C.J., Williams, G.P., Etemad, S., Dutta, B., DeRosa, F., Inam, A., Venkatesan, T., and Xi, X, 1990, "Fast Bolometric Response by High Tc Detectors Measured with Subnanosecond Synchrotron Radiation," *Appl. Phys. Lett.*, Vol. 57, pp. 2725-2727.

Chantry, G. W., 1984, *Long-wave optics : the science and technology of infrared and near-millimetre waves,* Academic Press, Orlando.

Chen, G., and Tien, C.L., 1992, "Partial Coherence Theory of Thin Film Radiative Properties," *J. Heat Transfer*, Vol. 114, pp. 636-643.

Chen, R.C., Wu, J.P., and Chu, H.S., 1995, "Bolometric Response of High-T_c Superconducting Detectors to Optical Pulses and Continuous Waves," *J. Heat Transfer*, Vol. 117, pp. 366-372.

Choi, B.C., Zhang, Z.M., Flik, M.I., and Siegrist, T., 1992, "Radiative Properties of Y-Ba-Cu-O Films with Variable Oxygen Content," *J. Heat Transfer*, Vol. 114, pp. 958-964.

Cunsolo, S., Dore, P., Lupi, S., Trippetti, R., Varsamis, C.P., and Sherman, A., 1993, "Infrared Conductivity of YBCO from Transmittance and Reflectance Spectra of Thin Films," *Physica C*, Vol. 211, pp. 22-28.

Fenner, D.B., Li, Q., Hamblen, W.D., Johansson, M.E., Hamblen, D.G., and Lynds, L., 1993, "Optical and Thermal Performance Advantages for Silicon Substrates in YBCO Bolometer Devices," *IEEE Trans. Appl. Supercond.*, Vol. 3, pp. 2104-2106.

Flik, M.I., Zhang, Z.M., Goodson, K.E., Siegal, M.P., and Phillips, J.M., 1992, "Electron Scattering Rate in Epitaxial $YBa_2Cu_3O_7$ Superconducting Films," *Phys. Rev. B*, Vol. 46, pp. 5606-5614.

Fork, D.K., Fenner, D.B., Barrera, A., Phillips, J.M., Geballe, T.H., Connell, G.A.N., and Boyce, J.B., 1991, "Buffer Layers for High-Quality Epitaxial YBCO Films on Si," *IEEE Trans. Appl. Supercond.*, Vol. 1, pp. 67-73.

Gao, F., 1992, *Temperature Dependence of Infrared and Optical properties of High Temperature Superconductors,* Ph.D. dissertation, University of Florida, Gainesville, Florida.

Gao, F., Carr, G.L., Porter, C.D., Tanner, D.B., Etemad, S., Venkatesan, T., Inam, A., Dutta, B., Wu, X.D., Williams, G.P., and Hirschmugl, C.J., 1991, "Far-Infrared Transmittance and Reflectance Studies of Oriented Thin Films," *Phys. Rev. B*, Vol. 43, pp. 10383-10389.

Gao, F., Carr, G.L., Porter, C.D., Tanner, D.B., Williams, G.P., Hirschmugl, C.J., Dutta, B., Wu, X.D., and Etemad, S., 1996, "Quasiparticle Damping and the Coherence Peak in $YBa_2Cu_3O_{7-\delta}$," *Phys. Rev. B*, Vol. 54, pp. 700-710.

Genzel, L., Bauer, M., Yoder, R., and Habermeier, H.-U., 1992, "Far-Infrared Investigations on $YBa_2Cu_3O_7$ Films with the Use of a Reflection Fabry-Perot Interferometer," *Solid State Communications*, Vol. 81, pp. 589-592.

Goldman, A.M., and Markovic, N., 1998, "Superconductor–Insulator Transitions in the Two-Dimensional Limit," *Physics Today*, Vol. 51, No. 11, pp. 39-44.

Griffiths, P.R., and de Haseth, J., 1986, *Fourier Transform Infrared Spectrometry*, John Wiley and Sons, New York, Chap.1.

Grischkowsky, D., and Keiding, S., 1990, "THz Time-Domain Spectroscopy of High T_c Substrates," *Appl. Phys. Lett.*, Vol. 57, pp. 1055-1057.

Grossman, E.N., 1989, "Optically Illuminated Dielectric Interfaces as High-Speed Far-Infrared Modulators," *Intl. J. Infrared and Millimeter Waves*, Vol. 10, pp. 803-820..

Grossman, E.N., and McDonald, D.G., 1995, "Partially Coherent Transmittance of Dielectric Lamellae," *Optical Engineering*, Vol. 34, pp. 1289-1295.

Hadni, A., Gerbaux, X., Cudraz, H.M., Tazawa, M., Mage, J.C., Marcilhac, B., Mercandalli, and Mansart, D., 1995, "Residual Losses of Superconducting Thin Films of $YBa_2Cu_3O_{7-\delta}$ in the Far Infrared and Microwaves: Applications," *Physica C*, Vol. 245, pp. 219-230.

Heavens, O.S., 1965, *Optical Properties of Thin Solid Films*, Dover Publication, Inc., New York, Chap. 4.

Kamarás, K., Herr, S.L., Porter, C.D., Tache, N., Tanner, D.B., Etemad, S., Venkatesan, T., Chase, E., Inam, A., Wu, X.D., Hegde, M.S., and Dutta, B., 1990, "In a Clean High-T_c Superconductor You Do Not See the Gap," *Phys. Rev. Lett.*, Vol. 64, pp. 84-87.

Karrai, K., Choi, E., Dunmore, F., Liu S., Ying, X., Li, Q., Venkatesan, T., Drew, H.D., Li, Q., and Fenner, D.B., 1992, "Far-Infrared Magneto-Optical Activity in Type-II Superconductors," *Phys. Rev. Lett.*, Vol. 69, pp. 355-358.

Klein, M.V., and Furtak, T.E., 1986, *Optics*, 2nd ed., John Wiley & Sons, New York, Chap. 5.

Komm, D.S., Blanken, R.A., and Brossier, P., 1975, "Fast-Scanning Far-Infrared Fabry-Perot Interferometer," *Appl. Opt.*, Vol. 14, pp. 460-464.

Kumar, A.R., Boychev, V.B., Zhang, Z.M., and Tanner, D.B., 1999a, " Fabry-Perot Resonators Built with $YBa_2Cu_3O_{7-\delta}$ Films on Si Substrates," To be presented at the *1999 International Mechanical Engineering Congress and Exposition.*

Kumar, A.R., and Zhang, Z.M., 1999, "Far-Infrared Spectroscopy of High-Temperature Superconducting Films on Silicon Substrates," in: *Recent Research Developments in Applied Spectroscopy*, S.G. Pandalai, ed., Research Signpost, India, Vol. 2, accepted for publication.

Kumar, A.R., Zhang, Z.M., Boychev, V.B., and Tanner, D.B., 1999b, "Temperature-Dependent Far-Infrared Absorptance of Thin $YBa_2Cu_3O_{7-\delta}$ Films in the Normal State," *Microscale Thermophysical Engineering*, Vol. 3, pp. 5-15.

Kumar, A.R., Zhang, Z.M., Boychev, V.B., Tanner, D.B., Vale, L.R., and Rudman, D.A., 1999c, "Far-Infrared Transmittance and Reflectance of $YBa_2Cu_3O_{7-\delta}$ Films on Si Substrates," *J. Heat Transfer,* accepted for publication.

Loewenstein, E.V., Smith, D.R., and Morgan, R.L., 1973, "Optical Constants of Far-Infrared Materials, 2: Crystalline Solids," *Appl. Opt.*, Vol.12, pp. 398-406.

Malone, C.G., Zhang, Z.M., Flik, M.I., and Cravalho, E.G., 1993, "Optimized Design of Far-Infrared Fabry-Perot Resonators Fabricated from $YBa_2Cu_3O_7$," *IEEE Trans. Appl. Supercond.*, Vol. 3, pp. 2852-2855.

Mechin, L., Villegier, J.C., Bloyet, D., 1997, "Fast and Sensitive Suspended YBaCuO Microbolometers Using Silicon separated by Implanted Oxygen Substrates," *Appl. Phys. Lett.*, Vol. 70, pp. 123-125.

Mechin, L., Villegier, J.C., Rolland, G., and Laugier, F., 1996, "Double CeO_2/YSZ Buffer Layer for the Epitaxial gowth of $YBa_2Cu_3O_{7-\delta}$ Films on Si (001) Substrates," *Physica C*, Vol. 269, pp. 124-130.

McKnight, S.W., Stewart, K.P., Drew, H.D., and Moorjani, K., 1987, "Wavelength-Independent Anti-Interference Coating for the Far-Infrared," *Infrared Physics,* Vol. 27, pp. 327-333.

Miller, D., Richards, P.L., Etemad, S., Inam, A., Venkatesan, T., Dutta, B., Wu, X.D., Eom, C.B., Geballe, T.H., Newman, N., and Cole, B.F., 1993, "Correspondence Between Microwave and Submillimeter Absorptivity in Epitaxial Thin Films of $YBa_2Cu_3O_7$," *Phys. Rev. B*, Vol. 47, pp. 8076-8088.

Mogro-Campero, A., 1989 "High-Temperature Superconducting Thin Films on Silicon," in: *Processing of Films for High T_c Superconducting Electronics* T.Venkatesan, ed., SPIE Proceedings, Vol. 1187, pp. 38-46.

Pechen, E.V., Vent, S., Brunner, B., Pruckl, A., Lipp, S., Linder, G., Alexandrov, O., Schutzmann, J., and Renk, K.F., 1992, "Far-infrared Fabry-Perot Resonator with High T_c $YBa_2Cu_3O_{7-\delta}$ Films on Silicon Plates," *Appl. Phys. Lett.*, Vol. 61, 1980-1982.

Phelan, P.E., Chen, G., and Tien, C.L., 1992, "Thickness-Dependent Radiative Properties of Y-Ba-Cu-O Thin Films," *J. Heat Transfer*, Vol. 114, pp. 227-233.

Phelan, P.E., Flik, M.I., and Tien, C.L., 1991, "Radiative Properties of Superconducting Y-Ba-Cu-O Thin Films," *J. Heat Transfer*, Vol. 113, pp. 487-493.

Phillips, J.M., 1996, "Substrate Selection for High-Temperature Superconducting Thin Films," *Journal of Applied Physics*, Vol. 79, pp. 1829-1848.

Pollack, D.D., 1990, *Physics of Engineering Materials,* Prentice Hall, Englewood Cliffs, N.J., Chap. 6.

Poole, C.P., Farach, H.A., and Creswick, R.J., 1995, *Superconductivity,* Academic Press, California, Chap. 1.

Quinlan, S.M., Hirschfeld, P.J., and Scalapino, D.J., 1996, "Infrared Conductivity of $d_{x^2-y^2}$-Wave Superconductor with Impurity and Spin-fluctuation Scattering," *Phys. Rev. B.*, Vol. 53, pp. 8575-8582.

Renk, K.F., 1992, "Far-Infrared Spectroscopy of High Temperature Superconductors," in *Studies of High Temperature Superconductors*, A.V. Narlikar, ed., Nova Science Publishers, New York, Vol. 10, pp. 25-62.

Renk, K.F., Betz, J., Schützmann, J., Prückl, A., Brunner, B., and Lengfellner, H., 1990, "Use of High T_c Superconductors for Far-Infrared Fabry-Perot Resonators," *Appl. Phys. Lett.*, Vol. 57, pp. 2148-2149.

Renk, K.F., and Genzel, L., 1962, "Interference Filters and Fabry-Perot Interferometers for the Far Infrared," *Appl. Opt.*, Vol. 1, pp. 643-648.

Rice, J.P., Grossman, E.N., and Rudman, D.A., 1994, "Antenna-Coupled High-T_c Air-Bridge Microbolometer on Silicon," *Appl. Phys. Lett.*, Vol. 65, pp. 773-775.

Richards, P.L., 1994, "Bolometers for Infrared and Millimeter Waves," *J. of Appl. Phys.*, Vol. 76, pp. 1-24.

Sanderson, R.B., and Scott, H.E., 1971, "High Resolution Far Infrared Interferometer," *Appl. Opt.*, Vol. 10, pp. 1097-1102.

Siegel, R., and Howell, J.R., 1992, *Thermal Radiation Heat Transfer*, 3rd ed., Hemisphere Publications, Washington, DC.

Tanner, D.B., and Timusk, T., 1992, "Optical Properties of High-Temperature Superconductors," in *Physical Properties of High-Temperature Superconductors*, D.M. Ginsberg, ed., World Scientific Publishing Co., Singapore, Vol. 3, pp. 363-469.

Vaughan, J.M., 1989, *The Fabry-Perot Interferometer*, Adam Hilger Publishers, Philadelphia, PA.

Varma, C.M., Littlewood, P.B., Schmitt-Rink, S., Abrahams, E., and Ruckenstein, A.E., 1989, "Phenomenology of the Normal State of Cu-O High-Temperature Superconductors," *Phys. Rev. Lett.*, Vol. 63, pp. 1996-1999.

Virosztek, A., and Ruvalds, J., 1990, "Nested-Fermi-Liquid Theory," *Phys. Rev. B*, Vol. 42, pp. 4064-4072.

Wiese, P., Riederer, X., Schutzmann, J., Gorshunov, B., Betz, J., and Renk, K.F., 1992, "Far-Infrared Fabry Perot Filter of High Transmission with High-T_c Superconductor Reflectors," *Intl. J. Infrared and Millimeter Waves*, Vol. 13, pp. 65-70.

Yeh, P., 1988, *Optical Waves in Layered Media*, Wiley Publications, New York, Chap. 5 and 7.

Zhang, Z.M., 1994, "Optical Properties of Layered Structures for Partially Coherent Radiation," in: *Proc. Tenth Intl. Heat Transfer Conf.*, G.F. Hewitt (ed.), Vol. 2, pp. 177-182.

Zhang, Z.M., 1998, "Far-Infrared Radiation Modulators Using High-T_c Superconductors," *J. Heat Transfer*, Vol. 120, pp. 24-29.

Zhang, Z.M., Choi, B.I., Le, T.A., Flik, M.I., Siegel, M.P., and Phillips, J.M., 1992, "Infrareed Refractive Index of Thin $YBa_2Cu_3O_7$ Superconducting Films," *J. Heat Transfer*, Vol. 114, pp. 644-652.

Zhang, Z.M., and Flik, M.I., 1993, "Predicted Absorptance of $YBa_2Cu_3O_7$/YSZ/Si Multilayer Structures for Infrared Detectors," *IEEE Trans. Appl. Supercond.*, Vol. 3, pp. 1604-1607.

Zhang, Z.M., and Frenkel, A., 1994, "Thermal and Nonequilibrium Responses of Superconductors for Radiation Detectors," *Journal of Superconductivity*, Vol. 7, pp. 871-884.

Zhang, Z.M., Kumar, A.R., Boychev, V.B., Tanner, D.B., Vale, L.R., and Rudman, D.A., 1998, "Back-side Reflectance of High T_c Superconducting Thin Films in the Far infrared," *Appl. Phys. Lett.*, Vol. 73, pp. 1907-1909.

Zhang, Z.M., Le, T.A., Flik, M.I., and Cravalho, E.G., 1994, "Infrared Optical Constants of the High-T_c Superconductor $YBa_2Cu_3O_7$," *J. Heat Transfer*, Vol. 116, pp. 253-257.

BIOGRAPHICAL SKETCH

Ravi Kumar was born in Andhra Pradesh, India. He moved to Hyderabad at the age of eight where he received his schooling and Bachelor of Engineering from Osamnia University. After working for a period of eight months in a mechanical tool manufacturing company he pursued graduate studies and received a master's degree from the Indian Institute of Technology (IIT), Bombay. At IIT, he worked on gas turbine blade cooling and the transport phenomena in porous medium. Beginning in January 1996, Ravi worked for an electric power generating company for a period of seven months. In the spring of 1997, Ravi came to University of Florida for his doctoral studies where he worked on the temperature-dependent radiative properties of materials and thin film optics.

Ravi enjoys learning and discussing socio-economical issues of his mother country India. A critical observer of the contemporary political affairs of the third world countries especially middle east Asia and the Indian subcontinent, Ravi strongly believes that the concept of religion has done a great harm to the development of these countries.

Ravi wishes to pursue a career in applied heat transfer technology and he can be reached at: arkumar_71@hotmail.com

I certify that I have read this study and that in my opinion it conforms to acceptable standards of scholarly presentation and is fully adequate, in scope and quality, as a dissertation for the degree of Doctor of Philosophy.

Zhuomin Zhang, Chairman
Assistant Professor of Mechanical
Engineering

I certify that I have read this study and that in my opinion it conforms to acceptable standards of scholarly presentation and is fully adequate, in scope and quality, as a dissertation for the degree of Doctor of Philosophy.

Jacob N. Chung

Jacob N. Chung
Eminent Scholar of Mechanical
Engineering

I certify that I have read this study and that in my opinion it conforms to acceptable standards of scholarly presentation and is fully adequate, in scope and quality, as a dissertation for the degree of Doctor of Philosophy.

DY Goswami

D. Yogi Goswami
Professor of Mechanical Engineering

I certify that I have read this study and that in my opinion it conforms to acceptable standards of scholarly presentation and is fully adequate, in scope and quality, as a dissertation for the degree of Doctor of Philosophy.

David W. Hahn
Assistant Professor of Mechanical
Engineering

I certify that I have read this study and that in my opinion it conforms to acceptable standards of scholarly presentation and is fully adequate, in scope and quality, as a dissertation for the degree of Doctor of Philosophy.

David B. Tanner
Professor of Physics

This dissertation was submitted to the Graduate Faculty of the College of Engineering and to the Graduate School and was accepted as partial fulfillment of the requirements for the degree of Doctor of Philosophy.

December 1999

M. J. Ohanian
Dean, College of Engineering

Winfred M. Phillips
Dean, Graduate School